POLITECNICO DI TORINO

Corso di Laurea in Ingegneria Biomedica

Tesi di Laurea Magistrale

Differential M wave estimation for different levels of contraction of the abductor pollicis brevis

Politecnico di Torino

Relatore
Prof. Luca Mesin

Co-relatori
Prof. Taian Vieira
Ing. Matteo Raggi

Candidati
Luca Sansone
Paolo Casarino

Luglio 2024

Abstract

This thesis investigates the differential M-wave responses generated by various populations of motor units (MUs) when activated during different intensity levels of voluntary contractions. The study aims to enhance the understanding of neuromuscular activation patterns by experimentally identifying how different MU populations contribute to the overall M-wave signal under controlled contraction conditions.

The experimental protocol involves the use of electromyographic (EMG) recordings and electrical nerve stimulation to investigate the M-wave contributions from distinct MU populations.

The results provide new insights into the recruitment strategies of motor units and their physiological implications, contributing to the broader field of neuromuscular research. This work has potential applications in clinical diagnostics, rehabilitation, and the development of biofeedback systems.

Contents

List of Figures

Chapter 1

Introduction to Neuro-muscular System

Brain and muscles work together allowing the human body to perform movement. They are connected by a network of specialized cells: neurons and muscle fibres, which are bound together to form the motor unit. Motor units are the basic functional elements of the neuro-muscular system, which is the main responsible for the body's motion and posture control. This introduction will provide an overview of the main aspects of this fundamental biological apparatus, with the purpose of giving a more comprehensive understanding of the study's aim, with reference to [1].

1.1 Nervous system

The nervous system is a complex structure of cells called neurons (Fig. 1.1). Their function is to transmit electrical and chemical signals in order to send motor commands to the target muscles and collect sensory inputs coming from receptors. The nervous system can be divided into two main parts:

- Central Nervous System (CNS): it consists primarily of the brain and the spinal cord. The brain is the largest cluster of neurons and it is housed inside the cranium; it integrates sensory information and directs motor responses. The spinal cord represents a pathway for signals between the brain and the rest of the body.
- Peripheral Nervous System (PNS): it is made of all the nerves and neurons outside the central nervous system. It relays information to and from the CNS and the rest of the body. The PNS can be further divided into the somatic nervous system (which controls voluntary movements and sensory perception)

and the autonomic nervous system (which controls involuntary functions like heartbeat, digestion, and respiration).

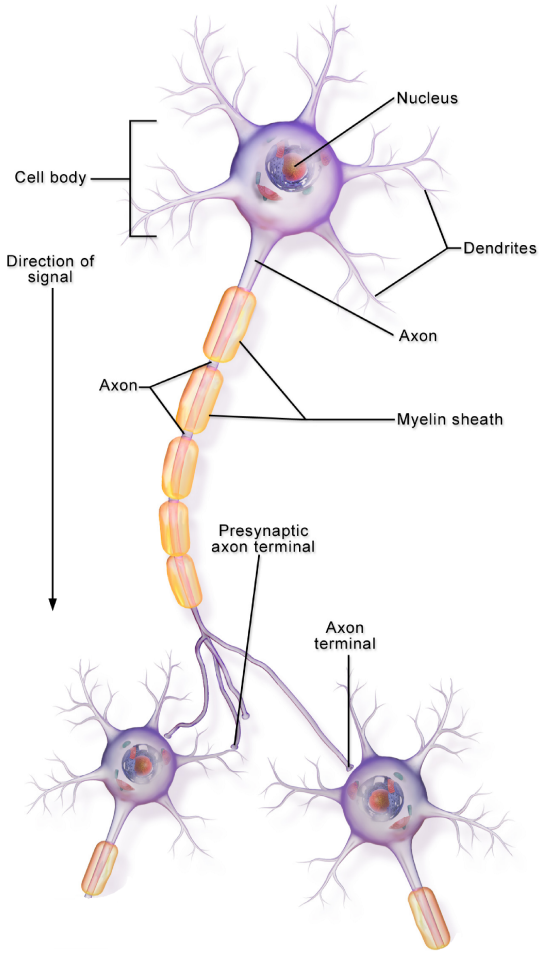

Figure 1.1: *Schematic representation of a neuron.*

Neurons are made of 3 principal parts:

- a cell body, which contains the nucleus and other cellular organelles;
- dendrites, that receive information from other neurons;
- an axon, that allows to send information to other neurons. The axons of the neurons can be covered with a particular lipid substance called myelin. It covers the axon and protects it, allowing a faster propagation of the electric impulse.

Nerve cells exchange information in the form of electrical and chemical signals with each other through particular connections called synapses. In particular, there are two kinds of synaptic junctions: electrical and chemical synapses. The first ones allow faster transmission of the electrical signal and they are characterised by the absence of gaps between the pre and the post-synaptic neuron. Instead, chemical synapses present gaps between neurons, in which the information propagates due to neurotransmitters that are released in the inter-synaptic space. As a result, the signal is converted into a chemical signal through neurotransmitters before being transformed back into an electrical signal and continuing its propagation.

1.1.1 Action Potential

The electric signal used by neurons to exchange information is called action potential (AP), represented in Fig. 1.2. The generation and propagation of action potentials depend on the cellular membrane and the distribution of ions both inside and outside the cell, particularly sodium (Na^+) and potassium (K^+) ions. In rest conditions, the concentration of these chemical species inside and outside the cell is not the same. Inside the cell, there is a higher concentration of K^+ ions, on the contrary, outside of the cell, there is a higher concentration of Na^+ ions. The difference in ion concentrations generates a voltage difference, called resting potential, which is approximately equal to -70 mV. This equilibrium potential is a weighted average of the Nernst potential of the different ions present in the cytoplasm and in the extracellular fluid, with weights depending on the membrane permeability to such ions. The Nernst equation is:

$$V_{eq} = V_i - V_e = \frac{RT}{zF} \ln \frac{c_e}{c_i} \tag{1.1}$$

where V_{eq} is the equilibrium potential, V_i and V_e are respectively the potential differences inside and outside the cell, R is the universal gas constant, T is the absolute temperature, z is the valence, F is the Faraday's constant, c the ion concentration [1].
The equilibrium potential is kept by the continuous activity of the Na^+-K^+ pump. The concentration gradient of each ion determines a flux across selective channels, that allows chemical species to pass through the cell membrane. These channels are voltage-dependent: their opening and closure depend on the voltage difference. The AP is a rapid change of the voltage of the cell membrane that undergoes a first depolarization followed by a re-polarization. All this process lasts approximately 5 ms. When the rest potential changes, in particular when it reaches the threshold value of -55 mV, selective Na^+ ion channels voltage-dependent open and a large amount of sodium ions enter the cell. Thus the difference voltage increases and it reaches values in the order of 30/35 mV. At this point, the re-polarization phase

begins since selective ion channels for potassium open allowing ions to leave the cell. At the same time, the ion channels for sodium close. During this phase, the cell undergoes an absolute refractory period throughout which it can't generate other APs. The absolute refractory is followed by a relative refractory period, a span of time when the neuron may produce a second AP if the stimulus received is strong enough. The voltage then reaches a lower value than the resting potential, reaching a condition known as hyper-polarization. Finally, the voltage returns to the value of -70 mV, the resting potential, thanks to the action of the sodium-potassium pump that restores the initial ion concentrations.

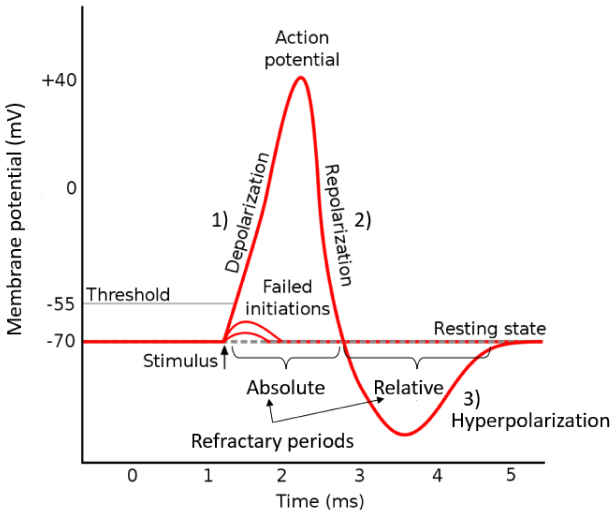

Figure 1.2: *Action potential phases: 1) depolarization, 2) repolarization 3) hyperpolarization.*

The Hodgkin-Huxley model

From an electrical point of view, many models have been proposed in the literature to explain action potential generation and propagation. Among them, the linear model of an excitable membrane presented by Hodgkin and Huxley, based on research conducted on the squid giant axon, describes quite faithfully what occurs in living organisms [2]. The electrical scheme of the model is shown in Fig. 1.3. The cell membrane can be seen as a parallel between a capacitor and several conductors with voltage generators, one for each ionic species that comes into play in defining the equilibrium potential. The modelled capacitor represents the intrinsic difference in the amount of electrical charge between the inside and outside of the cell. Conductors indicate the membrane channels' permeability to specific

ions, while voltage generators represent the tendency of each ionic species to reach its Nernst potentials. Finally, the current generators resemble the Na^+-K^+ pump.

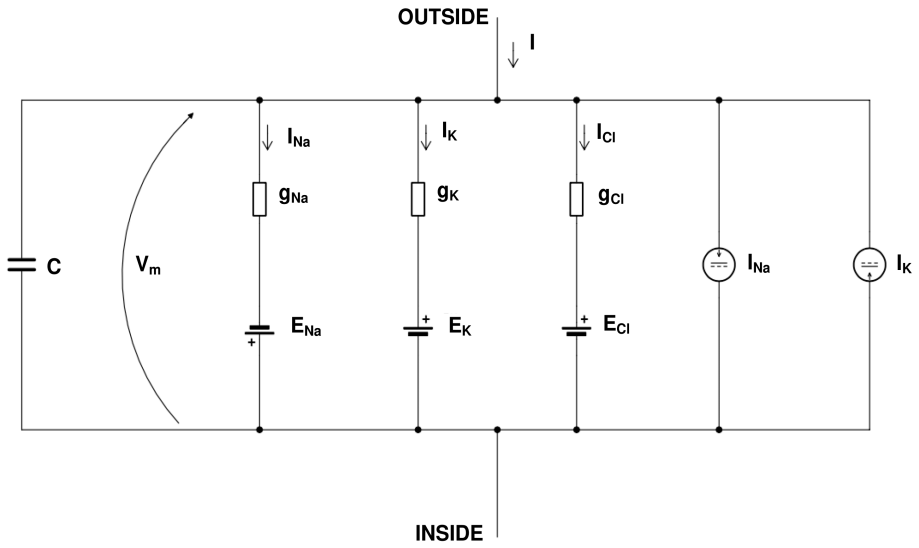

Figure 1.3: *Hodgkin and Huxley linear model: C represents the capacity of the membrane, g_i are the channels' conductivities and V_i are the Nernst potentials of ionic species. The current generators mimic the active pump.*

The Hodgkin-Huxley model accurately describes the behaviour of ionic channels during the onset of an action potential. The sodium channel has three sub-units of m type that activate the channel and one of type h that inhibits the channel. Therefore, the conductance of the sodium channel is described by the following equation:

$$g_{Na} = \bar{g}_{Na} m^3 h \tag{1.2}$$

where $\bar{g}_{Na}$ is a constant. At the same time, the conductance of the potassium channel can be modelled by:

$$g_K = \bar{g}_K n^4 \tag{1.3}$$

because it is formed by four independent sub-units of the same type, $\bar{g}_K$ is a constant factor. The m sub-units are characterized by faster dynamics than the h and n ones.
Assuming a linear model of the membrane potential given by only sodium and potassium, considering the previous equations 1.2 and 1.3 the equilibrium potential, in the rest condition, is defined as:

$$V_{eq} = \frac{g_{Na} V_{Na} + g_K V_K}{g_{Na} + g_K} \tag{1.4}$$

which is negative, because g_K is larger than g_{Na} and V_K is negative. Once the depolarization occurs, active sodium channels open, whereas inhibition gates stay closed. This causes the membrane potential to rapidly increase as positive feedback forces the activation gates for sodium to open. After some time, the inhibition gates close and potassium starts to exit the cell, causing the potential to return to a lower voltage, with a slower dynamic, hence the refractory period. By taking into account the chlorine ion, which is also responsible for action potential generation and propagation, the equation of equilibrium for the electrical current in Fig. 1.3 is:

$$c_m \frac{dV}{dt} + g_{Na}(V - V_{Na}) + g_K(V - V_K) + g_{Cl}(V - V_{Cl}) = 0 \tag{1.5}$$

This expression summarizes the model proposed by Hodgkin and Huxley.
In order to better mimic the complex processes that occur at a physiological level, several other solutions have been proposed in the literature. For example, the Goldman-Hodgkin-Katz equation is widely known to be a significant achievement in the field of electrophysiology [1].

Action potential propagation

Electronic conduction is the underlying mechanism that describes action potentials propagation in unmyelinated axons and muscle fibres [3].
The depolarization of the cell membrane generally affects only a limited section of the axon (Fig. 1.4). In this region, the membrane potential is reversed, with the inside of the cell being more positive than the outside. In adjacent areas, the resting potential remains negative, causing a flow of current inside and outside of the cell. Hence, the positive charges move towards the neighboring negative charges, thanks to the low resistance to ionic flows of the intra-cellular fluid. The currents induced by the movement of electric charges are strong enough to cause the depolarization of nearby regions, therefore the action potential propagates along the axon. The propagation occurs in only one direction because the refractoriness of the membrane prevents the action potential from going back.
Cable theory provides a mathematical explanation of this phenomenon [1]. Intracellular and extracellular axial currents can be described by a linear relation:

$$\frac{\partial V_e}{\partial X} = -r_e I_e \tag{1.6}$$

$$\frac{\partial V_i}{\partial X} = -r_i I_i \tag{1.7}$$

where r_e and r_i represent the resistance per unit length of the extracellular and intracellular media. Considering I_t as the total transmembrane current, Kirchhoff's law can be applied:

$$p(c_m \frac{\partial V}{\partial t} + I_{ion}) = I_t \tag{1.8}$$

where p is the perimeter of the axon and c_m is the capacitance of the membrane.

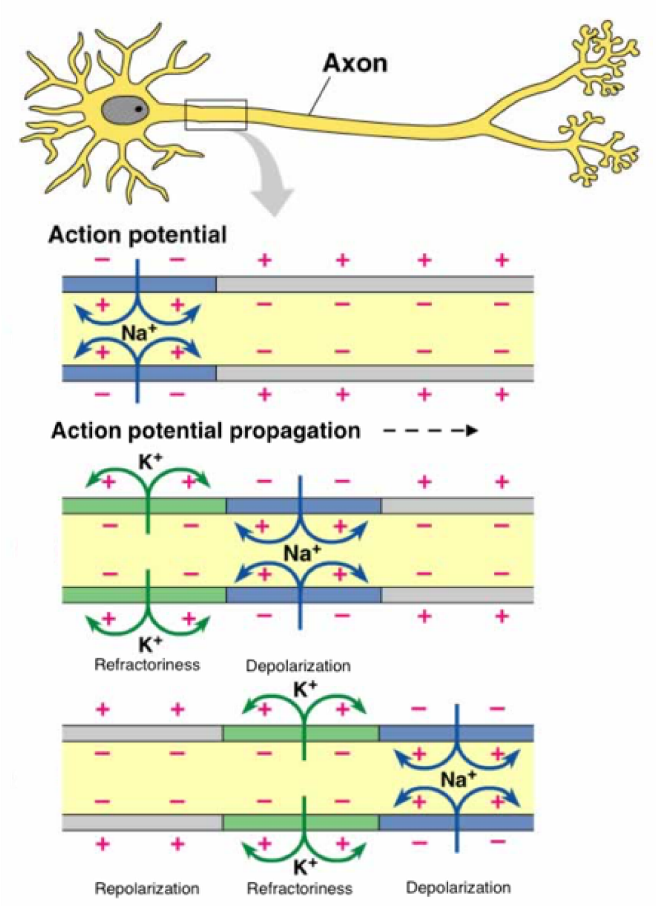

Figure 1.4: *Action potential's propagation along the axon of a motor neuron.*

The cable equation is obtained through the spatial derivative of the voltage:

$$\frac{1}{r_i + r_e}\frac{\partial^2 V}{\partial X^2} = p(c_m \frac{\partial V}{\partial t} + I_{ion}) \tag{1.9}$$

In axons coated with myelin sheath, the action potential is propagated through a process called saltatory conduction. The same mechanisms described above only apply to those parts of the membrane that are not covered in myelin, as it is resistant to ionic currents. These sites of the membrane are known as Ranvier's nodes and present a high concentration of voltage-gated channels for sodium and potassium. Ionic currents flow from one node of Ranvier to the next and do not pass through the myelin sheath, allowing faster potential conduction.

1.2 Muscolar system

The muscular system is made up of muscles and tendons. Muscles have the ability to contract, thereby producing force and causing motion.

1.2.1 Anatomy and physiology

Skeletal muscles are attached to bones through tendons. The connective tissue covering the tendon is called epimysium. Within the epimysium, another connective tissue divides the section of the muscle into numerous fascicles, each made up of thousands of muscle fibres. Muscle fibres are cells that extend along the entire length of the muscle and they are coated with a sheath called endomysium. These muscle fibres contain structures called myofibrils, which consist of thick myosin filaments and thin actin filaments, as shown in Fig. 1.5. Myofibrils are surrounded by the sarcoplasmic reticulum, a complex network of vesicles that is important in transmitting electrical impulses as well as in the storage of calcium ions. To serve this purpose, the reticulus is closely linked with structures known as transverse tubules or t-tubules.

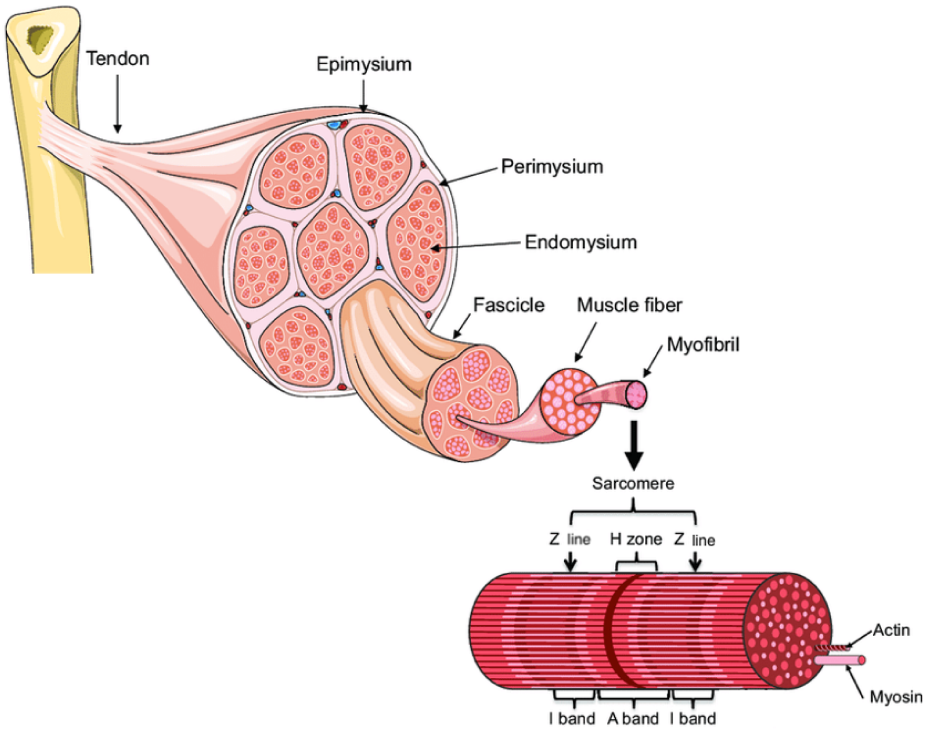

Figure 1.5: *Anatomy of a skeletal muscle.*

Actin is a globular protein that binds to itself forming a double helix structure. On the other hand, myosin is a dimer made up of two sub-units, whose ends consist of a tail and a head. Actin and myosin are contractile proteins that form sarcomeres within myofibrils. Z lines correspond to the boundaries between two sarcomeres, they are orthogonal to the longitudinal axis and hook the thin filaments at one end. Under a microscope, the sarcomere displays three distinct bands corresponding to different areas (Fig. 1.5). The A band is where thin and thick filaments overlap. At the center of the sarcomere, the H band can be observed, consisting only of thick filaments. Near Z lines, only thin filaments are present, forming the I band. In addition to actin and myosin, the myofibril filaments also present regulatory proteins: tropomyosin, an elongated protein, and troponin, which is a three protein complex.

1.2.2 Force production

Muscles are able to produce force through contraction. When a muscle contracts, thin actin filaments slide along thick myosin filaments. The sliding of the filaments occurs through a mechanism called the cross-bridge cycle [3].

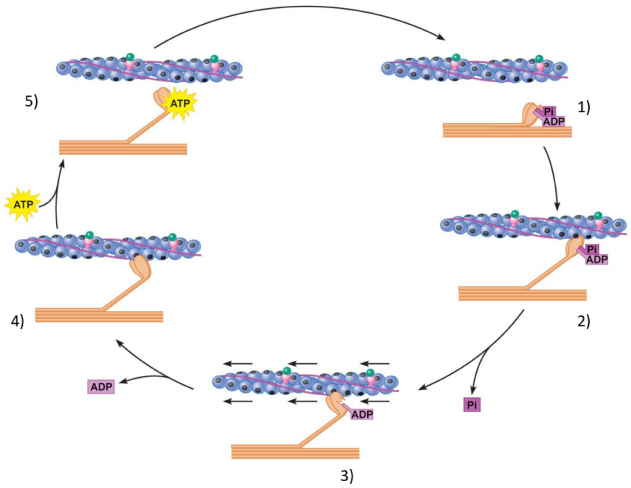

Figure 1.6: *Cross-bridge cycle: 1) myosin high-energy state 2) myosin-actin binding, 3) force pull, 4) myosin low-energy state, 5) myosin-actin detachment.*

In Fig. 1.6 the different steps of the cross-bridge cycle are shown. When ATP is hydrolyzed, it induces myosin to reach a high-energy state and bind with ADP and phosphate *(1)*. Once this state has been reached, myosin attaches to the actin in the presence of calcium *(2)*. Afterwards, the myosin head pulls the actin ligament towards the centre of the sarcomere *(3)*, after the detachment of inorganic phosphate (*(Pi)*). Then the ADP molecule is released from myosin that can reach

its low-energy state *(4)*. In this configuration, the muscle gets into a state of rigor. Finally, a new ATP molecule binds to the specific site on the myosin head *(5)*, causing it to separate from actin and return to its high-energy configuration.
Muscle contraction is typically investigated experimentally through three different modalities. One way is through an isotonic contraction, which occurs when the muscle must keeps a constant tension over time. During the effort, if the muscle shortens, the contraction is defined as concentric, whereas if the muscle is stretched, the contraction is defined as eccentric. On the other hand, the length of the muscle does not change during a isometric contraction. When the rate of change of the force produced is kept constant, the muscle performs an isokinetic contraction.

1.2.3 Fatigue

The force produced by the muscle naturally decreases after a prolonged period of time. This is due to muscle fatigue that comes into play in response to contractile activity. Muscle fatigue is usually caused by central and peripheral factors. Central fatigue is related to a decrease in the synchronization of motor neurons, while peripheral fatigue concerns the mechanism of action potential transmission at a muscular level.
The CNS adopts different strategies to cope with fatigue, that involve the recruitment of new motor units. Furthermore, central nervous system fatigue is also due to the decrease in the concentration of neurotransmitters available in the synapses. Meanwhile, peripheral fatigue is related to metabolic processes that occur in muscle cells.

Metabolic pathways in muscle cells

The energy required for muscle contraction is provided by ATP molecules. Muscle cells have an immediately available reserve of high-energy phosphates, which is found in the form of creatine phosphate. Once this reserve is depleted, there are two main metabolic pathways by which muscle fibres produce ATP. When physical activity is of moderate intensity, ATP production occurs through oxidative phosphorylation, in the presence of oxygen. If instead, physical effort is more intense, muscle cells produce ATP through glycolytic phosphorylation.
Oxidative muscle fibres produce energy following the first metabolic process. They are rich in mitochondria and typically have a small diameter. They are made of an oxygen-binding protein known as myoglobin, which confers them the red color. On the other hand, glycolytic fibres produce energy anaerobically through glycolysis. Pyruvate is produced as waste product, which is then transformed into lactic acid and accumulates in the extra-cellular environment.

An increase in the intensity of physical exercise causes an increase in the concentration of lactic acid in the muscle. Acidosis is a factor that influences the recovery from muscle-fatiguing exercise [4]. Furthermore, the waste products that result from glycolysis are removed from the environment by blood circulation; however, when a muscle contracts the pressure within the tissue increases, making it more difficult for the blood to reach the compartment. Therefore, lactic acid gathers more and more progressively over time, causing a slight feeling of pain and an increment in fatigue.

1.3 Motor Units

A single motor neuron innervates many skeletal muscle fibres. Individual motor axons branch within muscles to synapse on many different fibres that are spread over a relatively wide area, to ensure that the force is distributed evenly [5]. A motor unit (MU) consists of a motor neuron, the muscle fibres that it innervates, and the neuro-muscular junction, which is a synaptic connection between the two. This junction allows the transmission of action potential from the nerve to the muscle.

1.3.1 The neuro-muscular junction

Similar to neurons, muscle cells are capable of generating action potentials. The transmission of the electrical signal occurs across the neuro-muscular junction, represented in Fig. 1.7.
When an action potential travels down the axon terminal of an α-motor neuron, it causes the release of a chemical neurotransmitter, called acetylcholine, into the inter-synaptic space. Acetylcholine diffuses towards the membrane of the muscle cell and binds to specific receptors present on the motor end-plate, a region of the sarcolemma that is folded on itself to form a large number of inlets. The depolarization of the motor end-plate generates a large electrical signal, called end-plate potential. This signal spreads across the cell surface and triggers the release of Ca^{2+} ions from the sarcoplasmic reticulum. Ca^{2+} then attaches to the troponin, causing it to move along the actin filaments and expose the myosin binding sites. After the interaction between actin and myosin, the cross-bridge cycle occurs, which is explained in paragraph 1.2.2.

1.3.2 Motor units recruiment

Motor units differ in size. Typically, small motor neurons control only a few muscle fibres and form motor units that produce low forces, whereas large motor neurons innervate greater and more powerful motor units.

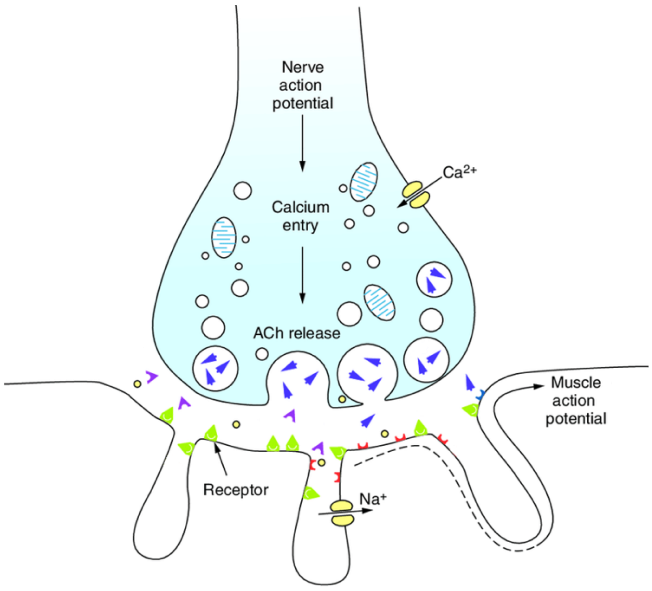

Figure 1.7: *An example of a neuro-muscular junction.*

Small motor units are composed of "red" muscle fibres, also known as type I fibres, that contract slowly and are fatigue-resistant. Larger motor neurons innervate larger "white" muscle fibres, called type II fibres, that generate more force; however, they tend to fatigue more rapidly.
When the central nervous system commands a target muscle to contract voluntarily, it implements very specific recruitment strategies that unfold over time and space. Spatial recruitment follows what is known as Henneman's rule: according to this principle, motor units are activated based on their size, from the smallest to the largest [6]. Each MU is characterized by a specific force threshold; once the effort needed for voluntary contracting a muscle exceeds this threshold, the motor unit starts firing at a certain frequency that increases along with the required force, until it reaches a maximum value; small motor units have generally lower thresholds. The several benefits of physiological recruitment are well described by Henneman's principle. Firstly, a precise generation of muscle forces can be obtained since smaller units, which are the first to be recruited, produce small twitches necessary to control fine motor skills. Secondly, motor neurons with large axons tend to innervate type II, less fatigue-resistant muscle fibres, whereas motor neurons with small axons tend to innervate type I, fatigue-resistant muscle fibres; in this way, a good efficacy against muscle fatigue is achieved.
Temporal motor unit recruitment concerns the frequency of activation of muscle fibre contractions. A single electrical impulse causes muscle fibres to produce a single force twitch. Since the duration of an action potential is shorter than the

duration of the force twitch, when the frequency of excitation of the motor units increases, the peak of the tension produced by the muscle rises until it reaches a maximum value. If the time of arrival of an action potential precedes the end of the previous stimulus, the force twitches add up over time. As the excitation of muscle fibres increases, the effort produced by the muscle reaches a plateau, known as tetanus.

Chapter 2

Electromyogram Detection

The APs of different MUs propagate along muscle fibres and generate a local potential difference in the excitable tissues around the muscle that can be recorded thanks to particular sensors called electrodes. An electromyogram (EMG) is the representation of this potential as a function of time. EMG can be detected with invasive and non-invasive techniques, depending on the electrodes used. Needle electrodes are used in the invasive EMG (needle EMG), for the other technique, surface electrodes are used and placed on the subject's skin, and for this reason, the last technique is also called surface EMG (sEMG). These two techniques have different characteristics.

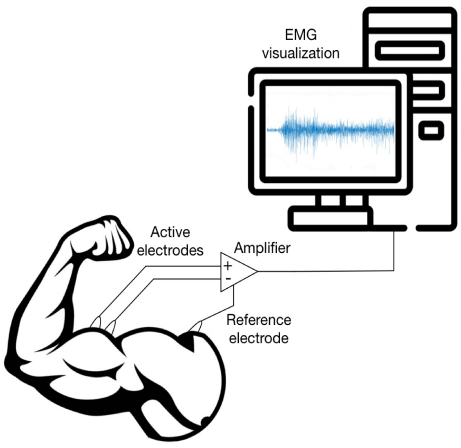

Figure 2.1: *EMG detection scheme. Note that the main components are present: active electrode, placed on target muscle, reference electrode, placed away from the target muscle, usually on bony prominences, the amplifier, the recording and visualization system and the EMG on the monitor.*

Needle EMG detects the signal from a small number of MU, those closest to the tip of the electrode. It has a small detection volume, approximately 1-2 mm^2. The amplitude range of this recorded signal is 0.1-5 mV and the frequency range is 0-10 kHz. Surface EMG detects the potential with electrodes placed on the subject's skin (Fig. 2.1). It has a bigger detection volume than needle EMG, and therefore, it detects the potential of a bigger number of MUs. The amplitude and the frequency ranges are respectively 50-2000 μV and 0.1-400 Hz. Surface EMG depends on the position of the electrodes concerning the muscle fibres, the materials of electrodes (the most used are in Ag/AgCl), and the distance between the electrodes, also known as inter-electrode distance (IED). The technique used in this project is sEMG.
As illustrated in Chapter 1, muscle contraction is triggered by currents of ionic species through the cellular membrane of elicitable cells. These currents can be generated by internal recruitment, driven by the central nervous system (CNS), but also by an external source of current. The latter case involves the use of a technique called electrical stimulation, in which an electrical current passes through the tissues, stimulating excitable cells.
The shape of the EMG changes depending on whether the subject performs a voluntary contraction or a stimulated contraction. In the first case (CNS recruitment), the signal has the shape of a stochastic process, and EMG manifests as an interfering signal (Fig. 2.2), in the second case, the signal is quasi-deterministic, because all different MUs recruited fire in the same time (Fig. 2.3).

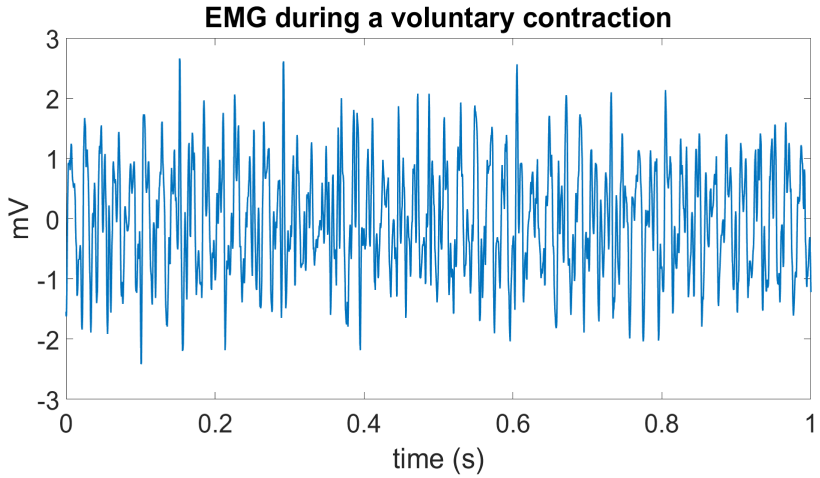

Figure 2.2: *Recorded EMG generated by a muscle voluntary contraction during the experimental protocol.*

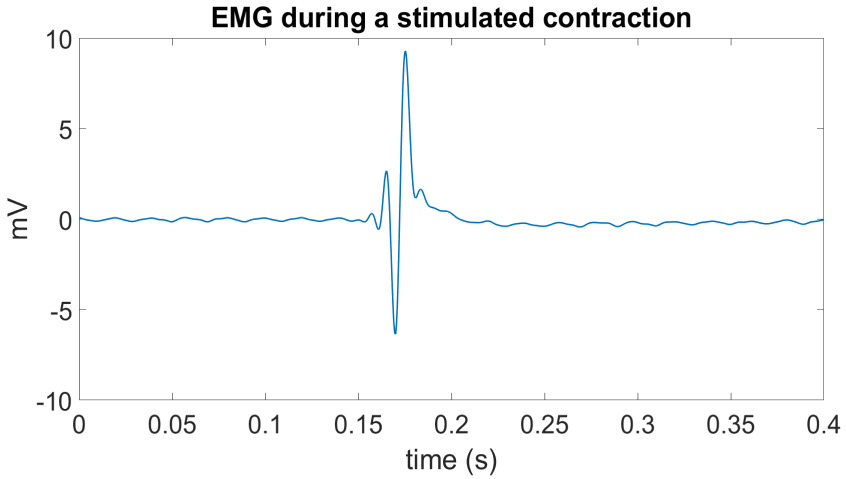

Figure 2.3: *Recorded EMG generated by a muscle stimulated contraction during the experimental protocol.*

2.1 Electrodes

To record the EMG signal is necessary to use electrodes (Fig. 2.4). In order to record a bio-potential, a pair of electrodes is used to measure the potential difference between two points on the human body. An electrode is a transducer, made of metal and an electrolytic solution, that allows the recording of the different potentials of the human tissues, generated by ionic currents that cross the cell membrane.

Figure 2.4: *Examples of surface electrodes.*

There are many aspects to consider in the connection between an electrode and the human skin. Human skin and the metal material conduct the current differently, thus they have different conductivities. Metallic materials are the materials with

the highest conductivity, while human skin conductivity is lower; furthermore, the way these two elements behave in terms of current conductivity is different. While metals, characterized by metallic bonding, conduct the current thanks to the free electrons present inside them, human skin conducts the electric current via ions: the electrode therefore manages to transform an ionic current that is present inside the human body into an electronic current that is present inside metal materials and vice versa [7]. In order to reduce those conduction differences, a conductive gel is usually placed between the skin and the electrode.
The skin can be represented as a solution containing ions and the electrode placed over it can be considered as immersed in an ionic solution. Therefore, when the electrode contacts the skin, oxidation-reduction reactions occur with the exchange of electrical charges between the metal and the solution. The metallic material releases positive metal cations into the electrolyte solution, freeing electrons that can move freely within the metal. The metal cations in the solution are deposited on the metal phase, binding to the negative surface charge. An equilibrium condition is therefore quickly attained. In this condition, the rate at which the metal loses cations, that oxidize when passing into solution, is equal to the deposition speed of metal ions on the surface of the electrode. These ions bind to the negative electric charges accumulated on the metal surface (Fig. 2.5).

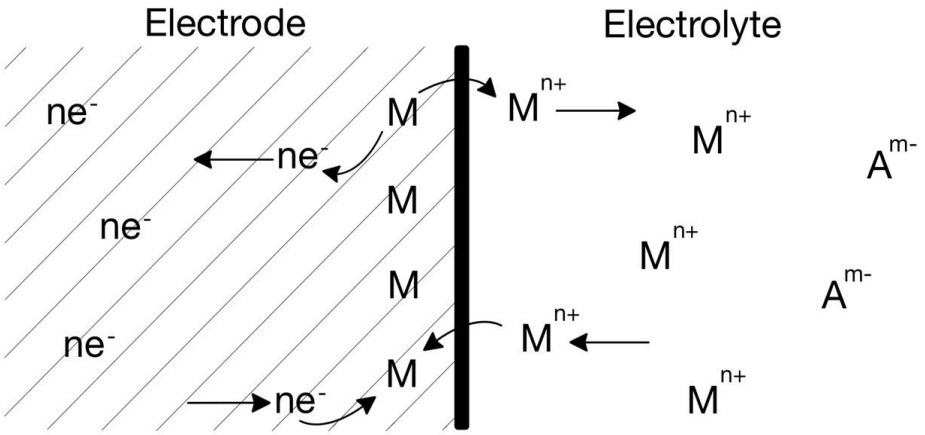

Figure 2.5: *Redox reaction at the electrode-electrolyte interface. Oxidation-reduction reactions take place at the interface between the metal electrode and the electrolyte. Some metal cations enter solution, leaving free electrons in the metal. At the same time, some cations metals present in the solution, bind to the negative charges present in the metal, leaving the solution and moving on the surface of the electrode. Note the presence of other species in the electrolyte solution in the form of anions.*

When this equilibrium is reached, the metal becomes negatively charged, while the electrolyte solution becomes positively charged. The following equation represents this equilibrium for a metal of valence n:

$$M \leftrightarrow M^{n^+} + ne^- \tag{2.1}$$

The charges are distributed at the interface between the metal and the solution, and an electrical double layer is therefore created, with a predominance of positive charges immediately outside the metal and a predominance of negative charges immediately inside of it (Fig. 2.6).

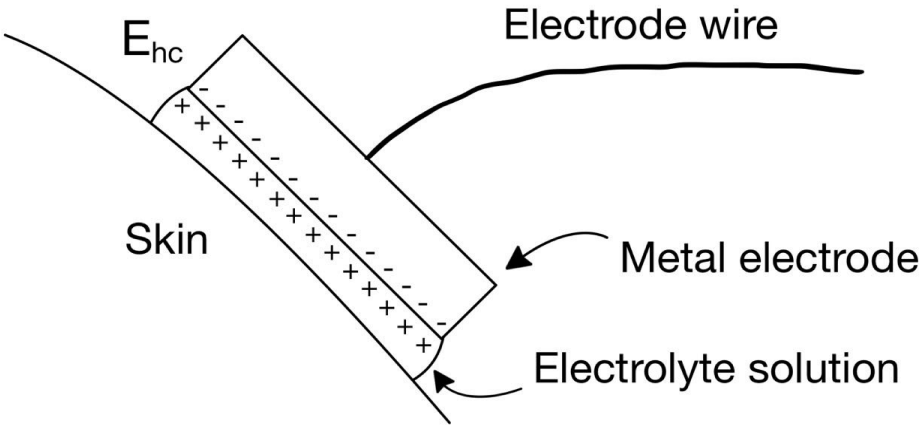

Figure 2.6: *Distribution of the electric charge at the electrode-electrolyte interface. At the interface, in an equilibrium condition, into the electrode there is an excess of negative charges, and into the electrolyte there is an excess of positive charges. This determines a potential difference called half-cell potential.*

The potential difference that is consequently created between the electrode and the electrolyte is called the half-cell or Nernst potential and is expressed by the following equation:

$$E_{eq} = E_0 + \frac{RT}{nF} ln \left[\frac{a_0}{a_r}\right] \tag{2.2}$$

where E_0 indicates the half-cell standard potential, R is the universal constant of gases, T is the absolute temperature in K, a_0 and a_r are the activity of the oxidized and reduced ionic species, n the number of electrodes of the reaction.
The electrodes can be divided into polarizable electrodes and non-polarizable electrodes. The perfectly polarizable electrodes allow the passage of current, without

causing the passage of charge: the behaviour of the double layer of charges that is created at the electrode/electrolyte interface is similar to that of the faces of a capacitor, in fact, these types of electrodes, in electrical diagrams, can be approximated by a capacitor. The perfectly non-polarizable electrodes allow the passage of current exclusively through charge exchange and can be approximated with a resistor. In general, an electrode can charge itself and simultaneously exchange charge with the surrounding solution, so its real behaviour is halfway between the two situations described above. For this reason, in an electric scheme, a real electrode is approximated with a capacitor placed in parallel with a resistor.
The most used electrode for EMG with these characteristics is the silver/silver chloride electrode (Ag/AgCl): metallic silver is covered with a porous layer of a specific salt of the same metal species (silver chloride). To complete the interface electrode-electrolyte's electric scheme, there is another element: the voltage generator in series with the parallel discussed before. This element represents the half-cell potential of the electrode, calculated with the Nernst equation (Eq. 2.2). Finally, we have to add a resistor placed in series with the previous element, that represents the bulk resistance of the gel (Fig. 2.7).

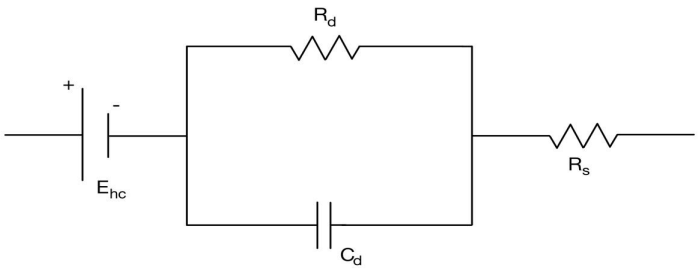

Figure 2.7: *Simplified electrode scheme.*

After the electrolyte paste, there is a layer of human skin, which is interposed between the electrode and the muscle that is the object of study, made up of excitable cells.
The skin is a complex tissue made up of three layers: epidermis, dermis, and subcutaneous layer. From an electric point of view, the two last layers are modelled by a resistor, while the first layer needs further explanation. It occupies the most important role, among the three layers, in the electrode-skin interface. It consists of three sub-layers in continuous renewal. In the deepest layer (stratum germinativum), closer to the dermis, the epidermis cells divide themselves, grow, and move outward until they reach the stratum granulosum, where they begin to die and

lose their nuclear material. They continue to move towards the outermost area: stratum corneum, in which they degenerate into layers of flat keratinous material. This layer is constantly being worn off and renewed by cells of the deeper layers. The epidermis is, thus, a constantly changing layer of the skin, and the outermost part, made up of dead cells, has different electrical characteristics compared to the deeper alive layers.
To obtain the complete electrical scheme of the electrode/skin interface, a model of the electrolyte/skin interface needs to be included [7]. The stratum corneum can be considered as a membrane semipermeable to ions, therefore variations in ionic concentrations across this membrane lead to the appearance of a potential difference, given by the Nernst equation. Moreover, the epidermal layer is also found to have an electric impedance that behaves as a parallel RC circuit, as seen for the electrode-electrolyte interface. The complete electrical scheme of the electrode/skin interface is shown in figure 2.8.

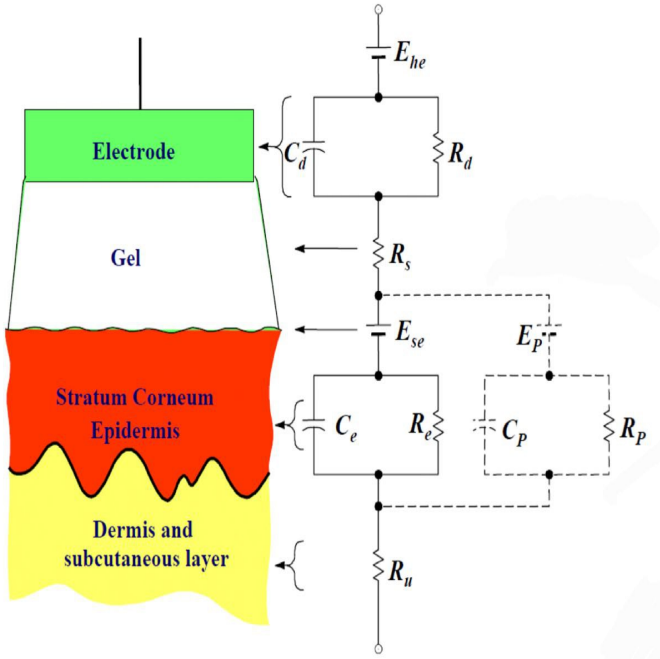

Figure 2.8: *On the left a summary diagram of the various layers from which the skin is composed and on the right the corresponding electrical diagram. The dotted components model the sweat glands and ducts.*

During electromyographic acquisitions it is desirable to minimize the effect of the stratum corneum to obtain better electrode-skin contact. An abrasive paste can be used to rub on the subject's skin to eliminate the stratum corneum or part of it.

Electric noise is an important problem during bio-potential acquisition and therefore also during EMG acquisition. It is necessary to reduce the noise because it can worsen the quality of the signal, making interpretation and subsequent processing difficult. Different sources can generate it, and based on the type of noise there are several techniques to reduce it. The most insidious type of electric noise is due to parasitic couplings with the powerline: parasitic impedances are created between the patient and the powerline and a current flows into the patient generating interference with the signal. Another type of noise is the so-called crosstalk: muscles close to the target muscle generate a signal that can be detected by electrodes placed on the target muscle. The motion of electrodes generates a destabilisation of the electrode-skin interface creating artifacts. Another source of noise is the stimulation artifact generated during the electrical stimulation. The electromagnetic sources and the variable electromagnetic field can represent two other important sources of noise. In the latter case, the variable electromagnetic field can generate a flux across a closed loop consisting of the electrode cables and the patient, which induces a current on them. This type of noise can be resolved by twisting the electrode cables in order to reduce the area of the closed loop.

2.2 Amplification chain for bio-potential

All biological signals, and therefore also the EMG, have a weak amplitude and thus require an amplification chain that allows their amplitude to be increased, in order to process, display, and record them. After the amplification, the signal is supplied as input to the analog-to-digital conversion block. The first block of the amplification chain is the front-end, made up of an instrumentation amplifier connected directly to the electrodes. Important parameters of this block are the input resistance and the CMRR (common mode rejection ratio). The first has a high value so as not to be affected by the filtering effect of the coupling of amplifier electrodes. Modern bio-potential amplifiers have an input impedance of at least 10 MΩ, which is sufficient to guarantee good signal quality. A good differential amplifier must greatly amplify the differential voltage, while it must not amplify the common mode voltage: a differential amplifier should have a high differential amplification compared to common mode amplification. The CMRR is defined as:

$$CMRR = 20 \log_{10} \left(\frac{A_d}{A_c} \right) \tag{2.3}$$

where A_d and A_c are respectively differential and common mode amplification.
A high-pass filter is often integrated into the front-end to eliminate noise resulting from the slow drifts or motion artifacts. The filter blocks serve to reduce or eliminate the noise. The differential signal output from the front-end is amplified and filtered. The last filter before the optoisolator block is a filter with an anti-aliasing function.

The cut-off frequencies for the high-pass and low-pass filters could be, for example, 10 and 500 Hz, respectively. It is rarer to find a band-reject filter to reduce any power line interference. Amplification and filtering blocks are appropriately alternated to avoid bringing the chain to saturation. To ensure patient safety, the part of the chain connected to the patient is isolated from the part connected to external devices via an optoisolator that is placed at the end of the amplification chain. The last block of the amplification chain is the analogue-to-digital converter (ADC). It serves to convert the analogue input signal into a digital quantity. The ADC samples the analogue signal with a sampling frequency that at least respects the Nyquist theorem. An ADC for a traditional amplification chain has a resolution of up to 16 bits. To obtain better resolutions a high-resolution ADC must be used, which can reach up to 24 bits and a more simplified amplification chain [7] [8]. A possible diagram of an amplified chain for EMG is shown in Fig. 2.9. Note in Fig. 2.9 the blue box at the bottom which contains an important circuit called driven right leg (DRL). The purpose of this circuit is to reduce the common mode component present at the input of the amplifier by lowering the impedance of the reference electrode.

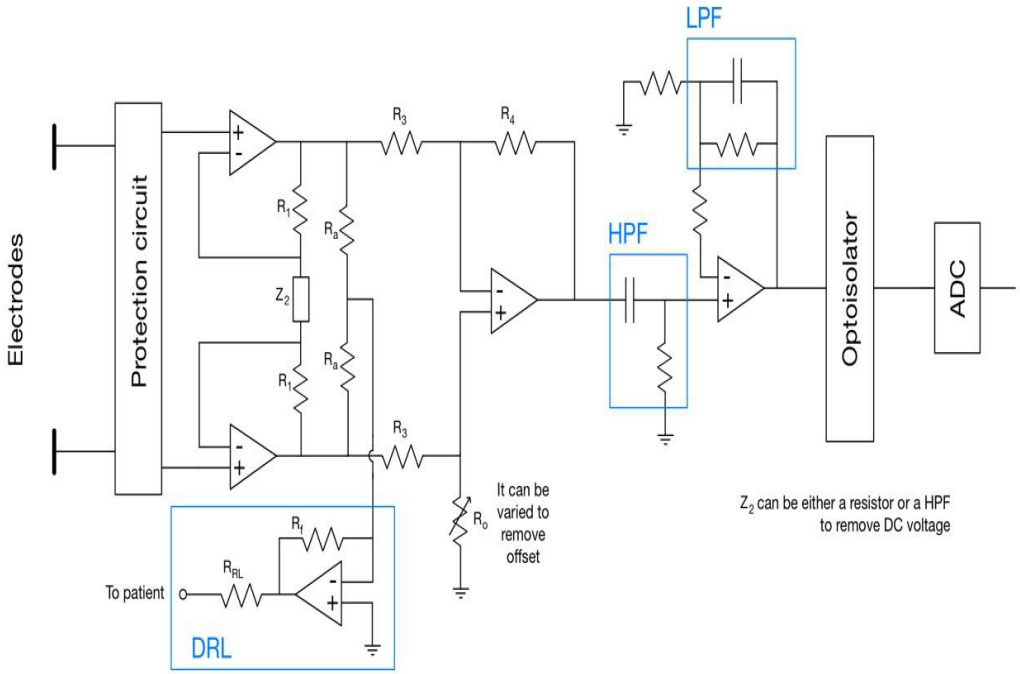

Figure 2.9: *An example of an amplified chain diagram for electromyography.*

2.3 EMG features

EMG features are important to extract and summarize information in both the time and frequency domains.

2.3.1 Amplitude indices

Amplitude parameters are important in evaluating muscle activation patterns. Surface EMG is an interference signal, its amplitude is the sum of all MUs that fire during a muscle contraction. This also depends on the position of the electrodes and the size and depth of the MUs. It is therefore important to summarize the information contained in the signal. The most common indexes in amplitude estimation are: *average rectified value (ARV)* and the *root mean square(RMS)*:

$$ARV = \frac{1}{N}\sum_{i=1}^{N}|EMG_{ch}(i)| \tag{2.4}$$

$$RMS = \sqrt{\frac{1}{N}\sum_{i=1}^{N}[EMG_{ch}(i)]^2} \tag{2.5}$$

where N is the number of samples of the considered epoch.
Thus, in order to calculate these indices, the signal is divided into epochs of approximately 100-500 ms [1].

2.3.2 Frequency indices

In addition to the amplitude indices, calculated in the time domain, the indices calculated in the frequency domain are important as well. Those indexes are computed on the *power spectral density (PSD)* of the signal. This quantity provides a frequency-based view of the EMG signal and it is linked to the firing frequency of the MUs [1]. There are two important strategies to estimate the PSD of a sampled signal through indirect and direct methods. To apply these strategies, the signal is usually divided in time epochs and each of them has to be wide sense stationary. To utilize the first method, it is necessary to calculate the auto-correlation function of the signal, and then, following the Wiener–Khinchin (WK) theorem, its Fourier Transform. Thus, to calculate the PSD with the indirect method, we have to apply the WK theorem and perform the Fourier transform of the auto-correlation function of the signal. It is known also by the name of correlogram method. The second strategy to perform the PSD is also called periodogram method. It consists of calculating the square of the Fourier transform of the signal. Periodogram and correlogram are not consistent estimators, and there are different ways to correct this limitation:

- The method of Daniell performs a moving average of sample spectrum.
- The method of Bartlett is based on dividing the signal into M epochs of K samples and on the average of the spectra of the different epochs. In this method, the epochs are not overlapped.
- The method of Welch is similar to Bartlett method, but unlike the previous case, the epochs can overlap (worsening resolution) and they are windowed (reducing the leakage and removing edge effects).
- The method of Blackman and Tukey tries to correct the limitations of the indirect method by windowing the auto-correlation function. This method considers only small delays, stabilizing the PSD estimate, but worsening the frequency resolution.

These methods lead to more robust estimators, through a smoothing procedure. From PSD estimation we can calculate important indices such as: mean frequency and median frequency, that can give important information on the firing frequency of MUs. The mean frequency is the barycentre of the spectrum and it is defined as:

$$MNF = \frac{\sum_{j=0}^{M} (f_j P_j)}{\sum_{j=0}^{M} (P_j)} \tag{2.6}$$

The median frequency is defined as the frequency that divides the power spectrum into two equal parts:

$$\sum_{j=0}^{N_{MDF}} P_j = \sum_{N_{MDF}}^{M} P_j = \frac{1}{2} \sum_{j=0}^{M} P_j \tag{2.7}$$

where, for both equations, P_j is the power spectral density of the EMG signal at a frequency bin j, M is the total number of frequency bins and N_{MDF} is the bin corresponding to the median frequency.

2.3.3 Conduction velocity

The AP propagates along nerve and muscle fibers with a speed known as conduction velocity (CV). It is an important parameter to estimate because it can give important information for example on fatigue of the muscle, on the type of fibers. Calculating the CV is theoretically simple because the AP on a single muscle fiber propagates with the same shape and in the same direction. It is therefore sufficient to have two detection points on the same fiber and knowing the inter-electrode distance (IED), it is possible to calculate the CV. However, CV estimation, in practice, is not so simple for different reasons:

- First of all, EMG is not a signal produced by a single muscle fibre, it is given by the sum of the different APs produced by the different motor units, present in the muscle, which are activated during the contraction and that fire with different frequency. Moreover, there are two different directions of propagation: from the innervation zone (IZ) towards two tendons. In a muscle there are several IZ. If the detection points are not placed between an innervation zone and a tendon, APs propagating in the opposite direction could cause a perturbation of the waveform.
- The detection system may not be aligned with the muscle fibers.
- The noise present during recordings could disturb the signal.
- Tissues are not homogeneous and do not all have the same conductivity, which may cause a change in the waveform of the signal.
- Non-propagating components, such as the end-fiber effect or the stimulation artifacts could produce a variation in the recorded EMG.
- If the muscle fibers are not parallel to the skin, as occurs in the pinnate muscles, CV estimation is more difficult.

There are different techniques for CV estimation based on single, two or more channels. The multi-channel techniques provide a more stable CV estimation, but they require EMG detection using arrays of electrodes (Fig. 2.10).

Figure 2.10: *An example of an electrode array.*

- **Scaling of the spectrum** It is a method based on a single channel. To perform this method, it is necessary to estimate the PSD of the signal and the mean frequency. The mean frequency is proportional to CV, with a proportional factor (α that depends on the volume conductor) [9]. The PSD of the signal can be approximated with the following equation:

$$P(f) = \frac{1}{v^2} G\left(\frac{f}{v}\right) \tag{2.8}$$

and thus the mean frequency can be written as:

$$MNF = \frac{\int_0^{+\infty} fG(f/v)df}{\int_0^{+\infty} G(f/v)df} = v\frac{\int_0^{+\infty} sG(s)ds}{\int_0^{+\infty} G(s)ds} = \alpha v \tag{2.9}$$

where v is the conduction velocity (CV), G is the shape of the spectrum and α is a term that depends on the volume conductor.

- **Spectral dips** This method also uses only one channel. Considering a single differential EMG detection, the PSD of the signal can be written as:

$$S(f) = M(f)\sin(\frac{\pi f d_e}{v}) \tag{2.10}$$

where $M(f)$ is the PSD of the monopolar signal, that propagates without distortion, d_e is the IED and v is the CV.
This function drops to zero when the sine function takes on the value zero. Therefore knowing the frequency of the dip and the inter-electrode distance (IED), CV can be estimated. It is not appropriate to use this method with small muscles because to make these dips more visible, we need to find them at lower frequencies. This is possible by increasing the IED [10].

- **Reference points** This technique is based on two detection channels and on the hypothesis that the signal detected by the first channel is the same detected by the second, shifted in time. The difference between the two channels is in the additive noise, which corrupts the two channels. This method consists of searching two reference points on the channels (for example zero crossing or local maximum or minimum points) and computing the delay between them. The disadvantage of this method is the finite sampling frequency, that determines the temporal resolution. With a traditional sampling frequency of 2 kHz and an IED of 5 mm, distinguishing between a CV of 5 m/s and a CV of 4 m/s (that are physiological CVs) is impossible. To improve this method you can oversample or interpolate the signals, close to the reference points.

- **Cross-correlation function method** Another technique based on two channels is the cross-correlation method. It must be computed the cross-correlation function between the two channels, whose maximum can give information on the delay between the signals. It is more stable to additive noise, but like the previous one, to obtain more reliable results, it's important to have a higher sampling frequency or an oversampling close to the maximum point.

- **Spectral matching** In order to perform this technique two channels are needed. The aim consists of minimizing the mean squared error of the two signals written as a function of the delay between them. The square error between the two signal can be written:

$$\int_{-\infty}^{+\infty} |x_1(t) - x_2(t-\tau)|^2 dt = \\ = \int_{-\infty}^{+\infty} |x_1(t)|^2 dt + \int_{-\infty}^{+\infty} |x_2(t-\tau)|^2 dt - 2\int_{-\infty}^{+\infty} |x_1(t)x_2(t-\tau)| dt \quad (2.11)$$

  The first terms on the right side of the equation are the energies of the two signals, the last is the cross-correlation function (multiplied by a minus sign). Applying Parceval equality and the properties of the shift, with the following equation, it's possible to move from the time domain to the frequency domain:

$$e^2(\tau) = \sum_{n=0}^{N-1} [x_1(n+\tau) - x_2(n)]^2 = \frac{1}{N^2} \sum_{k=0}^{N-1} |X_1(k)e^{j\frac{2\pi k\tau}{N}} - X_2(k)|^2 \quad (2.12)$$

  where N is the number of samples of the signal. This method is therefore based on finding the delay between the two signals in the frequency domain. It has the same advantages and disadvantages as the cross-correlation function method (explained above): it is stable to noise but it is sensitive to shape propagation of the potential. Moreover, it has no resolution problem because it works in the frequency domain in which the error function depends continuously on the delay τ.
  There are different strategies to minimize the error function. Two of the most popular are the gradient technique and Newton's technique.

- **Maximum likelihood estimation** This method belongs to multi-channel strategies: more than two channels are used to estimate the CV, in order to obtain a more consistent estimation.
  The multi-channel methods, summarized below, use the following signal model, assuming detected with an electrode array with equidistant electrodes:

$$x_k(n) = s(n - (k-1)\theta) + w_k(n) \quad (2.13)$$

where K is the number of available signals and $w_k(n)$ is an additive Gaussian noise. In order to compute the delay θ, the maximum likelihood estimation implies the minimization of the following error function:

$$e_{MLE} = \sum_{k=1}^{K}\sum_{n=1}^{N}[x_k(n) - \frac{1}{K-1}\sum_{m=1,m\neq k}^{K} x_m(n+\theta_{m,k})]^2 \tag{2.14}$$

It is a generalization of the spectral matching method. If only the relative distance between channels, which can be assumed to be the same, determines the relation between the delays, the maximum likelihood estimation can be evaluated, with constraints. However, the relationship can be rewrited in a more general way:

$$e_{MLE} = \sum_{k=1}^{K}\sum_{n=1}^{N}[x_k(n) - \frac{1}{K-1}\sum_{m=1,m\neq k}^{K} x_m(n+(m-k)\theta)]^2 \tag{2.15}$$

In this case, the maximum likelihood estimation does not have constraints, so $\theta_{m,k} = (m-k)\theta$. This method is useful when it is necessary to reduce the estimation variance significantly, for example, to appreciate small changes in CV over time.

- **Beamforming** Considering 2.15, it can be rewritten in the following way:

$$e_{MLE} = \sum_{k=1}^{K} e_k \tag{2.16}$$

where

$$e_k = \sum_{n=1}^{N}[x_k(n) - \frac{1}{K-1}\sum_{m=1,m\neq k}^{K} x_m(n+(m-k)\theta)]^2 \tag{2.17}$$

This method allows to compute the delay for which the mean square error between a reference signal and the other aligned signals is minimised. Beamforming is not optimum because a single channel is considered as a reference, thus not allowing the minimization of the variance. However, this method has advantages over MLE in non-ideal conditions, for example in case of misalignment between the muscle fibres and the electrode array [11].

Chapter 3

Electrical stimulation

Electrical stimulation consists in delivering external impulses to motor nerves in order to contract peripheral muscles, bypassing the central control of the nervous system.

3.1 Transcutaneous electrical stimulation

Depending on the electrode placement, transcutaneous electrical stimulation can be divided into neuro-muscular electrical stimulation and nerve stimulation.
Neuro-muscular electrical stimulation (NMES) has recently gained a lot of attention, due to its applications in the rehabilitation field [12], including muscle strengthening, maintenance of muscle mass and selective muscle training. An important use of electrical stimulation is a technique called FES (functional electrical stimulation), which is a treatment that involves the use of low-energy electrical pulses to artificially produce movement in paralyzed body limbs of subjects who have sustained injuries at the level of the central nervous system. Nerve stimulation has a primary application known as transcutaneous electrical nerve stimulation (TENS), a non-invasive method involving mild, high-frequency electrical impulses, whose goal is to alleviate chronic pain. Otherwise, nerve stimulation is mainly used for research purposes and clinical investigations, which is precisely the reason why it has been investigated throughout this study.
Different types of biological tissues are excited distinctively by external current pulses, which are characterized by two main parameters: rheobase and chronaxie. The rheobase is operationally defined as the minimal amount of electrical current of infinite duration needed to evoke an action potential in a cell, while chronaxie is defined as the minimum time required by a constant electric current, with an amplitude double the intensity of the rheobase, to induce a physiological response of the organism.

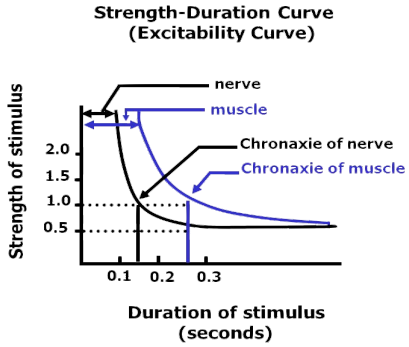

Figure 3.1: *Excitability curves: the muscle excitability curve is shown in blue and the nerve curve is shown in black.*

To successfully stimulate an excitable tissue, external electrical pulses must have values of duration and magnitude above a certain threshold; such threshold is described by the excitability curve, shown in Fig. 3.1. The excitability curve splits the graph into two portions: the intensity-duration pairs that fall within the right side of the curve are able to elicit a propagating action potential into a nerve or a muscle fibre, respectively.

3.1.1 The Hoffmann reflex and the M-wave

Neurons have similar excitability curves to muscle fibres; however, they slightly differ in terms of chronaxie and rheobase values. Low energy impulses of long duration (typically 1 ms) may selectively stimulate nerves over muscles, since sensory afferents usually have lower thresholds than motor efferents, resulting in a specific reaction called the Hoffman reflex. This reflex represents a long-latency response, due to the propagation of action potentials along afferent fibres from the stimulation point until they reach an α-motor neuron, as depicted in Fig. 3.2. The motor neuron then generates more action potentials traveling along efferent fibres until they reach the neuro-muscular junction and produce a twitch response in the electromyograph [13]. As stimulation increases, the amplitude of the H reflex increases until it reaches a maximum, and then decreases. At the same time a greater number of motor fibres is elicited by external current pulses, giving rise to the M-wave.
The M-wave is a compound muscle action potential (also known as CMAP), a signal that occurs due to the synchronization of motor unit firings following external stimulation. Many factors influence M-wave properties, including the number of active motor units (MUs), their size (larger units produce higher potentials than those generated by smaller ones), location (the contribution of deep MUs is more

attenuated than superficial MUs) and conduction velocity, the spread of neuromuscular junctions territory, the thickness of the subcutaneous layers, the relative orientation between recording electrodes and muscle fibres, and the morphology of intra-cellular action potentials [14].

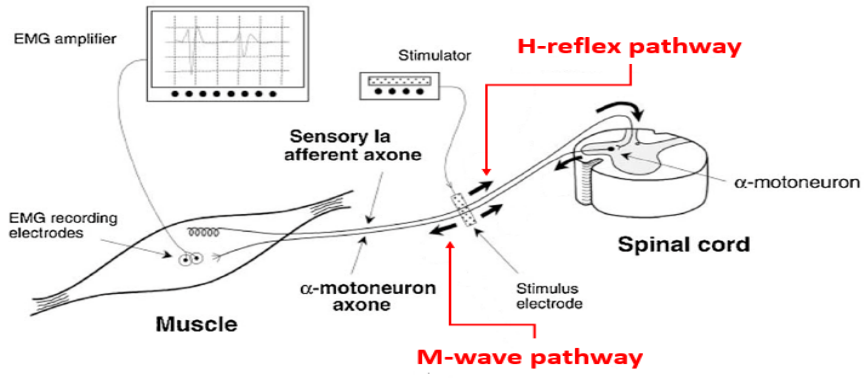

Figure 3.2: *Description of propagating action potentials along afferent and efferent pathways that result in the Hoffmann reflex.*

Both the Hoffmann reflex and the M wave are indicators of the excitability of motor units. Specifically, the H reflex is a diagnostic tool associated with specific neurological pathologies related to feedback circuits of the spinal cord, while the M-wave has been widely investigated for myoelectric fatigue considerations and motor unit number estimation methods.

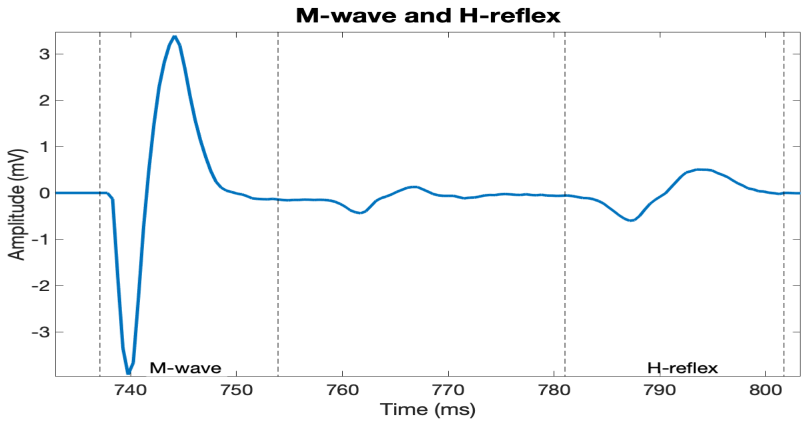

Figure 3.3: *M-wave and H-reflex from an EMG recorded during the experimental phase: M-wave is a short-latency response, while H-reflex can be observed typically 30-35 ms after the elicited M-wave.*

The Hoffmann reflex is delayed with respect to the M-wave and the latency changes according to the distance of the muscle to the spinal cord. Thus, it is possible to distinctly observe the two signals in a superficial EMG recording (Fig. 3.3).

3.1.2 Spatial recruitment of MUs

Voluntary contraction recruits motor units following the Hennemann's principle, as already discussed in paragraph 1.3.2.
Differently, the use of external stimulation implies that the recruitment order of the motor units no longer follows the Henneman rule. Since the usual order of recruitment is not respected, the strategies implemented by the central nervous system to cope with fatigue, like increasing the firing rate of motor units or the substitution of active motor units, cannot be applied. Therefore, protocols including electrical stimulation are more fatiguing over time.
Many studies have tried to explain how MUs are activated during transcutaneous electrical stimulation; most of them agree on the fact that a non-selective recruitment of motor units occurs when using NMES [15]. It is more likely that they are engaged by means of geometrical factors: superficial MUs are invested by a greater current density and are elicited more easily than deep MUs, regardless of their size.
Peripheral nerves that are triggered by external electrical current impulses are affected by a current density that is approximately equal across the diameter of different axons. Larger axons are invested by a greater electrical charge density and they activate before the smaller ones. This leads to a reversal of the recruitment order: fast-twitch muscle fibres of type II are recruited prior to slow-twitch fibres of type I.
The differences in motor unit recruitment between the two different configurations (voluntary contraction and nerve stimulation) were considered as initial hypotheses for the development of the study.

3.2 Monopolar and bipolar stimulation

The electrodes used to deliver the electrical stimuli differ, depending on two parameters: size and type of electrode-skin interface. The selectivity of electrodes depends on their size, while their conductivity is determined by the interface with the skin, see section 2.1.
Electrical pulses are delivered in two different configurations that differ in electrode placement: monopolar and bipolar stimulation. Before applying the stimulation electrodes on the subject it is necessary to search for the motor point. The motor point represents the area of the skin above the muscle where the motor threshold is the lowest for a given electrical input [16].
Monopolar stimulation is a technique that typically implies the use of a small active

electrode and a larger reference electrode placed on opposite sides of the target muscle (Fig. 3.4a). The stimulation current is injected from the active electrode, flows through the tissue and closes its loop on the reference electrode. Therefore, superficial axons are invested by a greater amount of density current and can be elicited selectively. In this configuration is of primary importance to position the active electrode on the motor point of the muscle, since the cone of current affects a specific region of the volume.

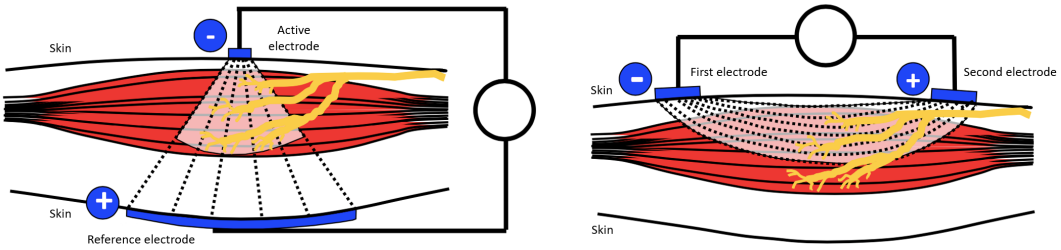

(a) *Monopolar stimulation* **(b)** *Bipolar stimulation*

Figure 3.4: *Electrode placement in monopolar and bipolar stimulation: in monopolar stimulation (a) electrodes are placed on opposite sides, on the other hand in bipolar stimulation (b) electrodes are positioned on the same side.*

Bipolar stimulation is implemented by placing the electrodes on the same side of the muscle, resulting in a banana-shaped path for the injected current (Fig. 3.4b). This type of stimulation affects a larger targeted volume and results in a more effective muscle contraction. While electrode placement is not as crucial as in monopolar stimulation, proper positioning facilitates a good physiological response.

3.3 Stimulator

The device used to deliver electrical current pulses is a stimulator consisting of a user interface that enables the setting of amplitude, duration, and frequency of the stimulation pulses, and an output stage. The output stages of electrical stimulators may be classified into three main groups :

- constant voltage output stage;
- constant current output stage;
- hybrid output stage.

Each configuration has its own advantages and disadvantages [17] that will be discussed in the following.

Ideally, the aim is to obtain a user-settable output current and a sufficiently rapid voltage drop that does not hinder the recording of the acquired signal.

3.3.1 Voltage driven stimulator

An electrical stimulator that is voltage-driven allows to control the output potential of electrical pulses (Fig. 3.5a). The amplitude, duty cycle, and frequency of the voltage can be set by the user. However, the current that flows through the muscle is unknown because it is also determined by the impedance of the tissue with the skin (Fig. 3.5b). Nevertheless, a voltage-driven electrical stimulator is relatively easy to make and has the advantage of attenuating the stimulation artifact component, due to the fast decay of the potential over time.

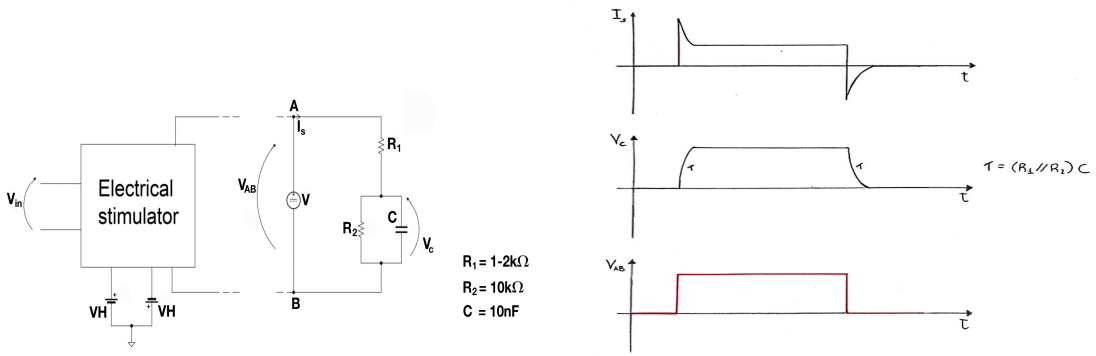

(a) *Voltage driven stimulator output stage* **(b)** *Trend of parameters over time*

Figure 3.5: *Voltage driven stimulator: (a) represents the electrical scheme, (b) shows the resulting output current and voltage.*

3.3.2 Current driven stimulator

To solve the problem of not being able to determine the current flowing through the subject, it is possible to use a current-driven stimulator (Fig. 3.6a). With this solution, the user can choose the characteristics of the output current, even if the output potential of the pulses varies over time (Fig. 3.6b). As long as the stimulator can provide the necessary voltage, the current does not depend on the tissue impedance. However, the main issue of this solution is related to the stimulation artifact, as the voltage decay is slower and the artifact may overlap with the elicited M-wave.

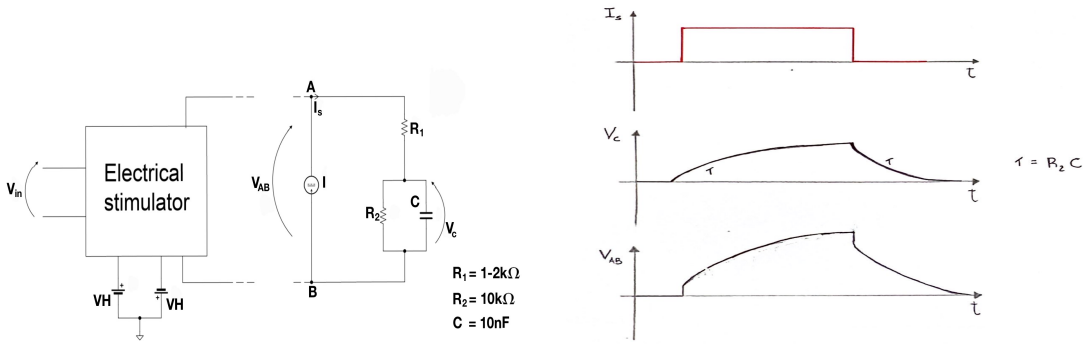

(a) *Current driven stimulator output stage* **(b)** *Trend of parameters over time*

Figure 3.6: *Current driven stimulator: (a) represents the electrical scheme, (b) shows the resulting output current and voltage.*

3.3.3 Hybrid stimulator

Delgado and Del Pozo [18] proposed a new solution, a hybrid stimulator, that combines the advantages of the two previous designs (Fig. 3.7a). This system allows users to set the parameters of the desired current for the electrical pulses and reduces the stimulation artifact (Fig.3.7b). Before applying stimuli to the subject, the system behaves as a current-driven stimulator, as represented in Fig. 3.4a with the switch opened. At the end of stimulation, the switch closes, and the system becomes a voltage-driven stimulator that imposes null voltage.

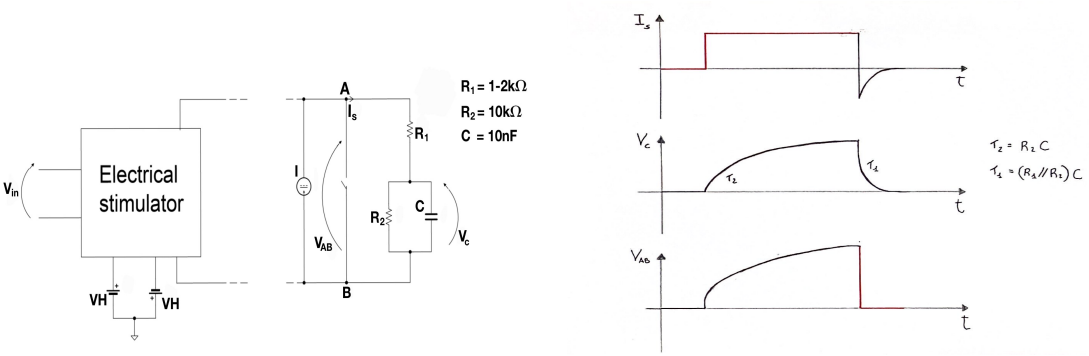

(a) *Hybrid stimulator output stage* **(b)** *Trend of parameters over time*

Figure 3.7: *Hybrid stimulator: (a) represents the electrical scheme, (b) shows the resulting output current and voltage.*

3.4 Stimulus Artifact

During electrical stimulation of a peripheral nerve, external pulses evoke a potential that is recorded by the system of detection and may interfere with the recorded M wave (Fig. 3.8). This stimulus artifact must be removed in order to accurately investigate the electrophysiolgical response.
The stimulation artifact represents a noise component, visible on the electromyogram as a high-frequency positive peak, that appears a few milliseconds from the moment the stimulus is delivered. The extent of the amplitude of the artifact depends on several factors [1]:

- intensity of the stimulus;
- shape of the stimulus;
- output stage of the stimulator;
- electrode-skin impedance.

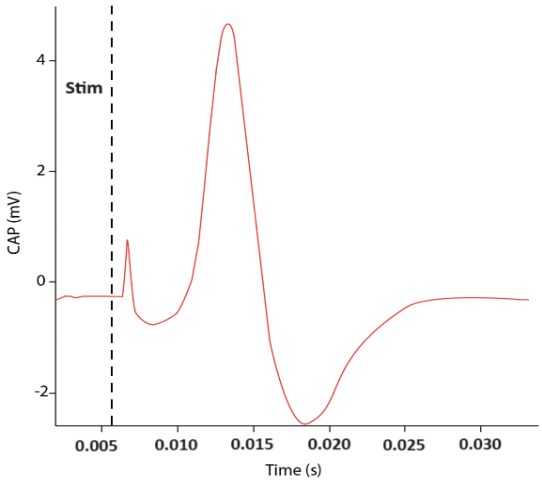

Figure 3.8: *Example of a sùtimulus artifact from an EMG tracing.*

Different measures can be taken into account for the removal of the stimulus artifact, both from a hardware and software perspective. As discussed in the previous section, the voltage-driven stimulator is more effective than the current-driven stimulator in terms of artifact reduction. Good care should be taken while placing the electrodes as the application of a conductive gel between them and the skin results in a low

impedance and hence, in a decrement of the stimulus artifact. Also, the artifact increases linearly with the level of stimulating current and decreases as the distance between the detection system and the stimulation point becomes larger [19].
There are two main hardware solutions that are implemented to minimize the stimulus artifact: the blanking circuit and the slew limiter. The first one imposes a null voltage at the input of the amplifier for a brief period after the stimulation, while the latter prevents rapid variations in potential from occurring. However, these measures may not be sufficient to completely remove the noise, so several software techniques can be found in the literature:

- **Adaptive blanking**

  The adaptive blanking technique consists of putting to zero the first samples of the signal after the on-set stimulation. In order to properly identify the portion of the signal to be investigated, the mean frequency of the signal (MNF) must be calculated. Due to the fact that the stimulus artifact is a high-frequency noise, by setting its samples to zeros, the MNF of the overall signal decreases, and the number of data that should be deleted is denoted by the minimum value of this parameter, see section 2.3.2.

- **Adaptive filtering**

  Adaptive filtering implies the estimation of the stimulus artifact with a neural network, starting from a model. If the estimator correctly reconstructs the artifact it is then subtracted from the signal. This solution has an issue due to the relatively short duration of the stimulus artifact, which is typically less than a few samples with normal sample frequencies.

- **M-wave reconstruction**

  To solve the problem of adaptive filtering technique, it is possible to reconstruct the M-wave instead of the stimulus artifact. The advantage of this approach is that M-wave is defined in many more samples, making its estimation more accurate. The modeled M-wave may be the signal recorded from the furthest electrode away from the point of stimulation, since this recording channel should be less affected by the stimulation.

Chapter 4

Materials and methods

The purpose of the thesis project is to estimate the differential M-wave of MUs that fire at different force levels. The study was carried out on the abductor pollicis brevis, a muscle of the hand (in particular of the thumb), which is part of the group of muscles located in the thenar eminence (Fig. 4.1).

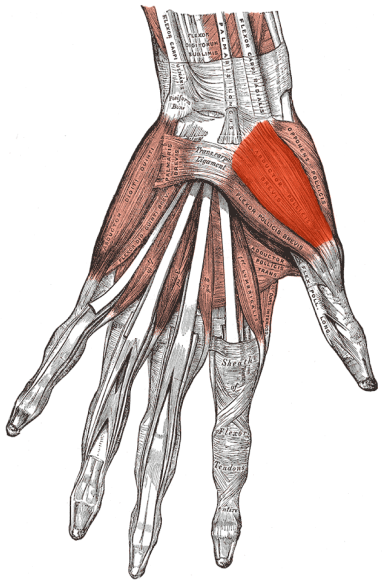

Figure 4.1: *Palmar view of the hand muscles with particular emphasis on the target muscle: the abductor pollicis brevis.*

When it contracts, it flexes and abducts the metacarpophalangeal joint of the thumb [20]. It is innervated by the median nerve which runs along the entire upper limb up to the hand. After the carpal tunnel, it separates into several branches, one of which innervates the muscles of the thenar eminence and also the target

muscle of this study: the abductor pollicis brevis [21].

4.1 The rationale behind the study

The idea behind the study is to superimpose a stimulated contraction on the voluntary contraction in order to recruit two different sets of MUs of the same muscle.
Firstly, through a voluntary contraction, following Hennemann's principle [6], as force increases, the MUs are recruited based on their size, in particular, the smaller ones are recruited first, and then the larger diameter ones are also recruited. When the muscle expresses its maximal voluntary contraction (MVC), all the MUs are recruited. Therefore, by imposing an appropriate sub-maximal mechanical stimulus on the muscle, it is possible to recruit, through a voluntary contraction, part of the MUs, in particular, the MUs with smaller diameters (Fig. 4.2a).
On the other hand, when electrical stimulation is applied to the nerve, the MUs are recruited according to the intensity of the electrical current. At low intensities, larger MUs are recruited, while as the intensity increases, the smaller MUs begin to be elicited.
If the intensity of electrical stimulation is high enough all the MUs of the muscle are recruited. This situation is reached by injecting a supra-maximal current (SMC) into the nerve. Therefore, only the MUs with larger diameters are recruited by stimulating with a sub-maximal current (Fig. 4.2b). These two orders of recruitment are both non-linear: a 50% MVC contraction does not correspond to a 50% recruitment of the MUs, and similarly, the same considerations are valid during stimulated contraction.
It is possible to record the muscle response through electromyography, and when the electrical stimulation is superimposed on the voluntary contraction, an M-wave is detected, in correspondence with the electrical impulse, typically visible over a background EMG. During low-level contractions, far from the MVC (such as at 20% MVC), only the MUs with smaller diameters are recruited. When electrical stimulation is superimposed to the voluntary exercise with an intensity lower than the SMC (such as at 50% SMC), both smaller motor units, through voluntary contraction, and larger motor units, through electrostimulation, can be recruited. Therefore, the MUs with intermediate diameters may not be recruited (Fig. 4.3a). By keeping the current intensity constant, as the level of contraction increases, the intermediate MUs are also recruited by the CNS, until reaching the point where all the MUs are recruited: the small and intermediate ones by the voluntary contraction and the large ones by the electrical pulse. In this case, the M-wave should remain constant, because it is given by the same MUs, while the background EMG should have a greater intensity because more MUs are recruited by CNS (Fig.

4.3b).

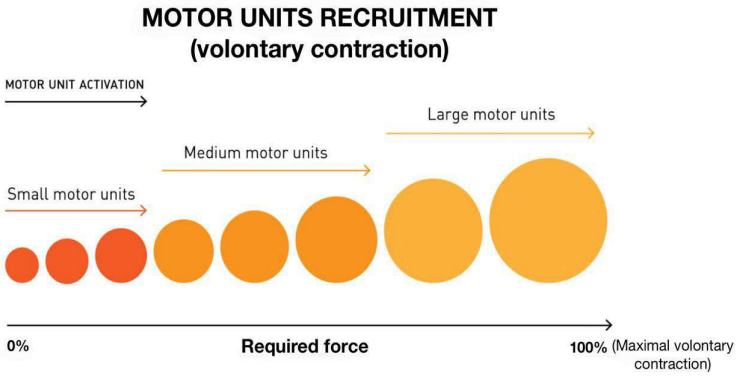

(a)

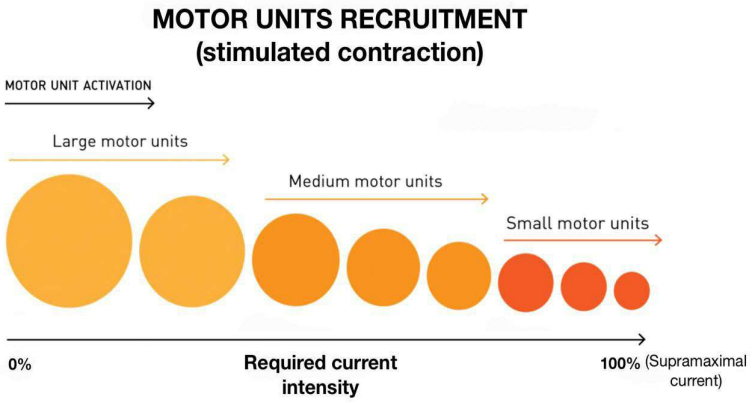

(b)

Figure 4.2: *(a) scheme of MUs recruitment during a voluntary contraction (b) scheme of MUs recruitment during a voluntary contraction.*

By further increasing the contraction level, the CNS recruits part of the MUs

that were previously recruited by the electrical stimulus, and when the stimulus arrives, those MUs are in a refractory period, thus they should not contribute to generating the M-wave, but they should contribute to increasing the intensity of the background EMG: in this case, there is a change of the waveform of the M-wave, with an amplitude reduction (Fig. 4.3c).

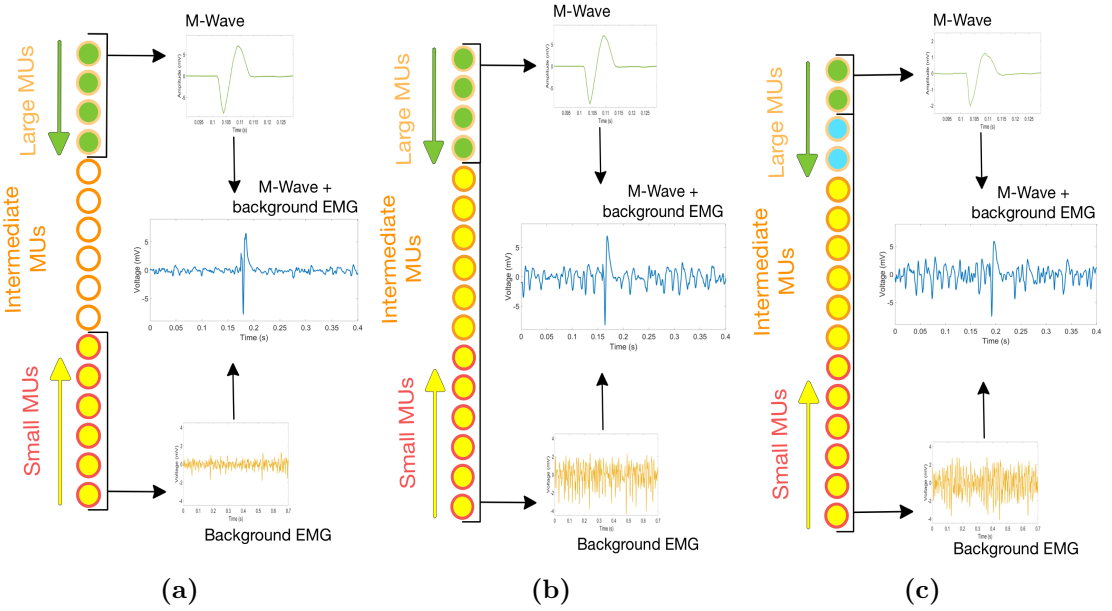

Figure 4.3: *The figure shows how the recruitment of MUs occurs while a stimulated contraction overlaps with a voluntary one. The motor units depicted in yellow are recruited by the CNS and are responsible for generating the background EMG, while the green ones are recruited by the electrical stimulus and are responsible for the M wave. The yellow and green arrows indicate the direction of recruitment. Note that the current intensity remains constant from left to right, while the voluntary contraction increases. The EMG signal of the MUs recruited by the CNS increases, while the M-wave remains constant until it decreases in (c). In this last image, the MUs in blue are recruited by the CNS and therefore are in a refractory period when the stimulus arrives and this causes a reduction in the amplitude of the M-wave. The EMG signal is computed by the sum of the M wave and the background EMG.*

When the stimulation levels are closer to the SMC and the process is repeated, the point of overlap of the MUs recruited by the CNS and those recruited by the stimulus should shift towards lower contraction levels, because the stimulus recruits increasingly smaller motor units, therefore the M-wave relating to the MUs recruited by the stimulus should change shape at a lower level of contraction. In this way, it should be possible to estimate the M-wave related to the MUs that

are recruited by the electrical stimulus at a lower contraction level and that are in a refractory period when the stimulus arrives at a higher contraction level, thus the M-wave related to the MUs that are activated from one level of contraction to another.

4.2 Measuring force device

In order to proceed with the experiment it was necessary to measure the force (measured as a percentage of the MVC) generated by the target muscle during its contraction. To achieve this goal, a functional measuring device was designed with a software and realized for the required exercises of the experimental protocol, along with an acquisition system for the force signal. To designed this measure device was used Autodesk Inventor Professional 2024 [22].
To measure the force of the muscle a load cell (capacity of $10kg$) [23] was used and connected to an *Arduino UNO* [24] board for the display and the acquisition on a PC.
The measuring device (Fig. 4.4) consists of a platform on which to rest and stabilize the hand and an adjustable support on which the load cell is positioned. The subject's wrist was placed and stabilized on the latex support (see Fig. 4.4) and the thumb had to contact the load cell in order to abduct it and generate force. The load cell support was designed so that it could be adjusted in both directions of the plane, and in this way, the measuring device could better adapt to the different anatomical characteristics of the subjects. The subject can also use a support against which to press with the other fingers of the hand in order to perform the correct movement. The force signal produced by the contraction of the considered muscle is amplified, sampled and digitized by a 24-bit analog-digital converter called *HX711*, specific for interfacing the load cell with an acquisition board, as seen in (4.5). In this case, the Arduino Uno board was used as an acquisition board to process the output signal from the HX711 and send it to the computer to be able to acquire and display it. The software used to program Arduino was *MATLAB* [25]. Thanks to specific add-ons available online [26], it allowed to programming Arduino board to acquire and display the force signal, applied on the load cell, in real-time.
During acquisitions, it is important to synchronize the EMG signal with the force signal. This can be achieved by putting it as input to the EMG amplifier, which requires an analog input, while the force signal in output from HX711 is digital. Therefore, it is necessary to convert the force signal from digital to analog [27]. The force signal is output from the Arduino by driving a particular digital pin capable of generating PWM (pulse-width modulation) signals: digital signals with a variable *duty cycle* (DC) based on the voltage ranging from 0 ($DC = 0\%$) to $5V$

($DC = 100\%$). The voltage changes based on the force applied by the muscle on the load cell: $0V$ corresponds to zero force and $5V$ to the maximum force (in this case $10kg$).

Number	Description	Quantity
1	Principal structure	1
2	First load cell support	1
3	Second load cell support	1
4	Thumb contact	1
5	load cell	1
6	Sponge principal structure	1
7	Sponge thumb contact	1
8	Wrist support	1
9	Bolt M10x100 mm	2
10	Screw M4x16 mm	4
11	Washer 10 mm	2
12	Nut M10	2
13	Bush 10,1x12 mm	1

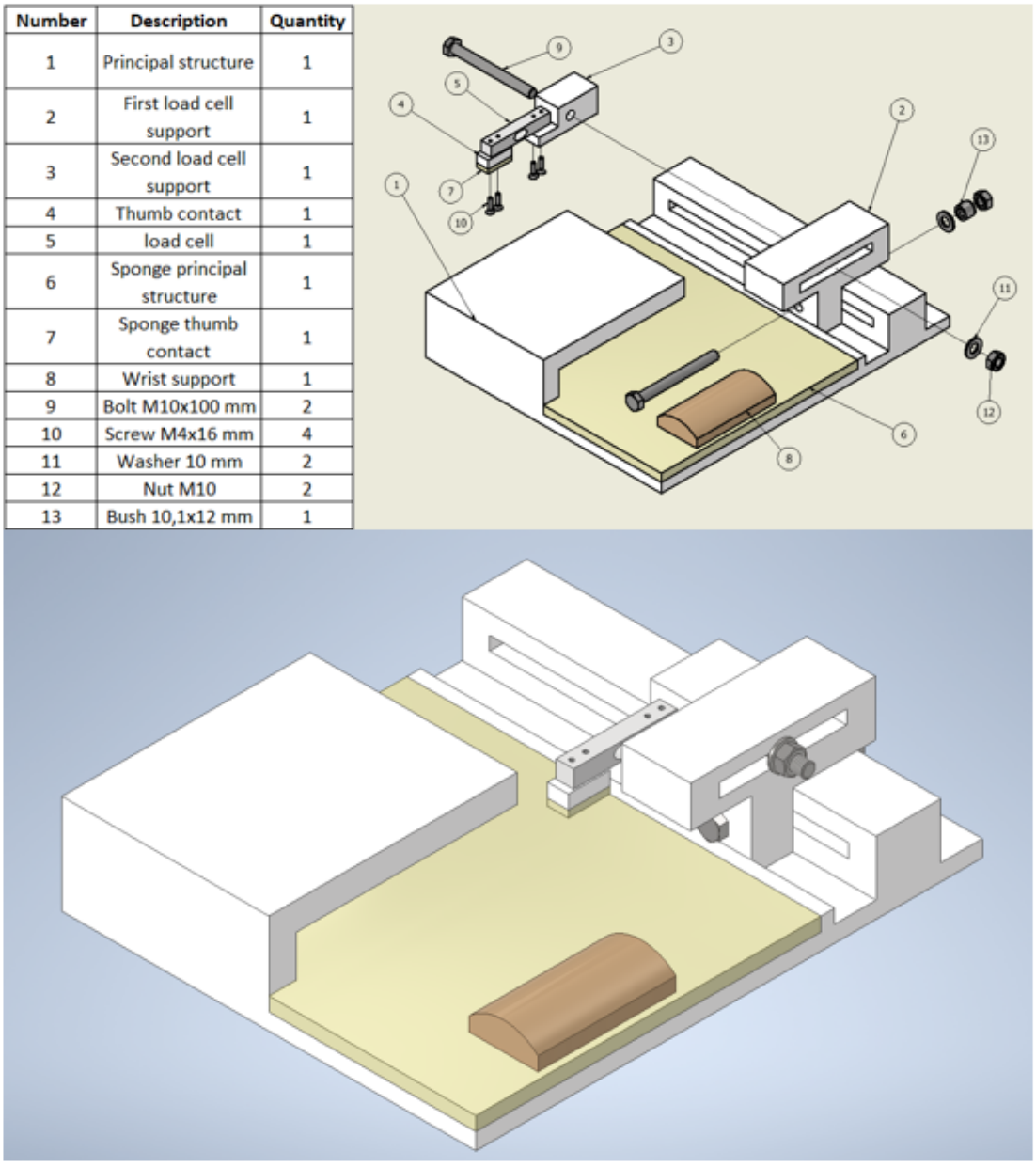

Figure 4.4: *Measurement instrumentation's exploded view (top right) with the table of components (top left) and 3D representation (down).*

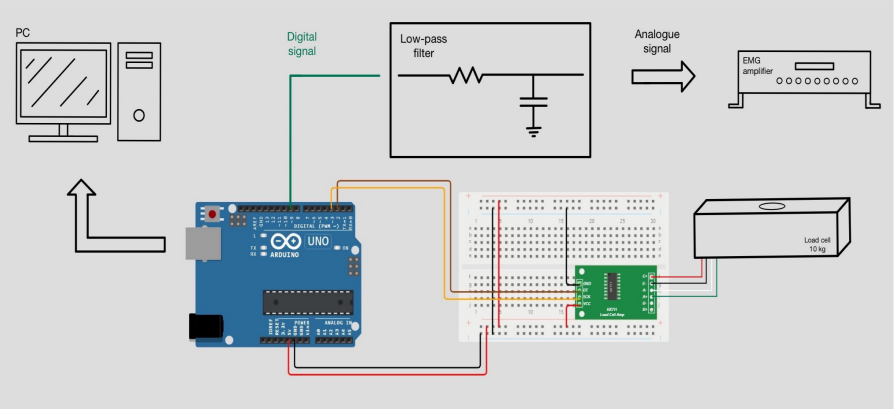

Figure 4.5: *Connection between the load cell, the Hx711 amplifier and the Arduino UNO board. The force signal reaches the EMG amplifier after a low-pass filter.*

4.3 Simulation model

A simulation model has been developed to enhance the hypotheses concerning the firing pattern of the motor units. The model was proposed by Fuglevand in 1993 [28], it comprises three elements: a motor neuron model, a model of motor-unit force, and a surface EMG model. For the purpose of the study, only the rate coding model of a motor neuron pool has been properly exploited.

4.3.1 Motor neurons recruitment

Simulated motor neuron recruitment is determined by two parameters: the excitatory drive (E) and the recruitment threshold excitation (RTE). The excitatory drive is the sum of action potentials received by the motor unit, while the recruitment threshold excitation is defined as the minimum E level required to start repetitive discharge in a motor neuron [28]. All motor neurons are elicited by the same amount of excitation drive. However, the values of RTE are assigned so that many neurons have low thresholds and few neurons have high excitation thresholds. The recruitment threshold excitation for the i-motor neuron is defined by:

$$RTE(i) = e^{ai} \tag{4.1}$$

in this expression a is a coefficient equal to:

$$a = \ln(RR)/n \tag{4.2}$$

RR represents the range of recruitment expressed as a percentage of the maximum voluntary contraction (MVC), while n indicates the number of motor units. The

number of motor units was set at 100 [29], and their range of recruitment was set to vary between 50-60 %MVC [30]. Larger motor neurons were assigned a higher conduction speed than smaller motor neurons.
The firing patterns of motor neurons are influenced by several factors, including the minimum firing rate (MFR), the E-firing rate relation, the peak firing rate, and the variability in the inter-spike intervals (ISIs) during steady-state excitation. The minimum discharge rate was the same for each motor neuron, and was set at 7 Hz [31]. Following Fuglevand's work, the firing rate of a motor neuron was modeled to increase linearly when the increment in excitatory drive surpasses the RTE:

$$FR_i(t) = g_e[E(t) - RTE_i] + MFR \qquad E(t) \geq RTE_i \tag{4.3}$$

where g_e is a gain, kept constant for all motor units. Each motor unit was restricted to a maximum firing frequency of 40 Hz [32]. To simulate the stochastic nature of motor neuron discharge, a certain variability of intervals between spikes has been taken into account. ISIs were distributed normally around the predicted mean interval, which can be computed from the previous equation:

$$\frac{1}{(t_{ij} - t_{ij-1})} = g_e[E(t) - RTE_i] + MFR \tag{4.4}$$

therefore:

$$ISI_{ij-1} = t_{ij} - t_{ij-1} = \mu + \sigma \cdot Z \tag{4.5}$$

This relationship allows to obtain random values of the inter-spike intervals, making the simulation more generalizable.

4.3.2 EMG simulation

EMG was then obtained by adding the MUAP trains (obtained by convolution of the firing patterns with MUAPs simulated for each UM). EMG patterns combined voluntary contractions with electrical stimulation. The level of stimulation was determined by the number of motor units recruited, while the excitatory drive factor represents voluntary contraction. Six different levels of force were considered: 10%, 20%, 30%, 40%, 50% and 60% MVC. Since nerve stimulation recruits large motor neurons, a simultaneous spike was imposed to activate a different number of motor units, depending on the level of stimulation. Voluntary contraction, on the other hand, activates muscle units depending on their size, following Henneman's principle.
The refractoriness of muscle fibers was considered by forcing that they could not produce a spike for the following 5 ms after the previous [33]. Furthermore, nerve stimulation can generate antidromic collisions which occur with a certain probability. The probability of an axon being refractory at the time of the stimulus depends on

the likelihood of an action potential having passed through the stimulation site prior to the stimulus [34].

$$P_{refr} = \frac{\frac{2d}{cv} \cdot \frac{f}{V\sqrt{2\pi}}}{(\frac{1}{f} - t_{refr}) \cdot \frac{f}{V\sqrt{2\pi}} + 0.5} \tag{4.6}$$

d represents the distance between the site of stimulation and the spinal cord, which was considered equal to 0.65 m. CV is the conduction velocity of the motor axon. t_{refr} is the refractory period and f is the mean firing frequency of the unit. V is a coefficient representing the variation of interspike intervals.
EMG patterns were obtained by convoluting the firing patterns and a single differential action potential propagating in a subcutaneous conductive volume. To ensure the consistency of the results, the EMGs were simulated with 20 different stimuli, and then averaged and filtered (Fig. 4.6).

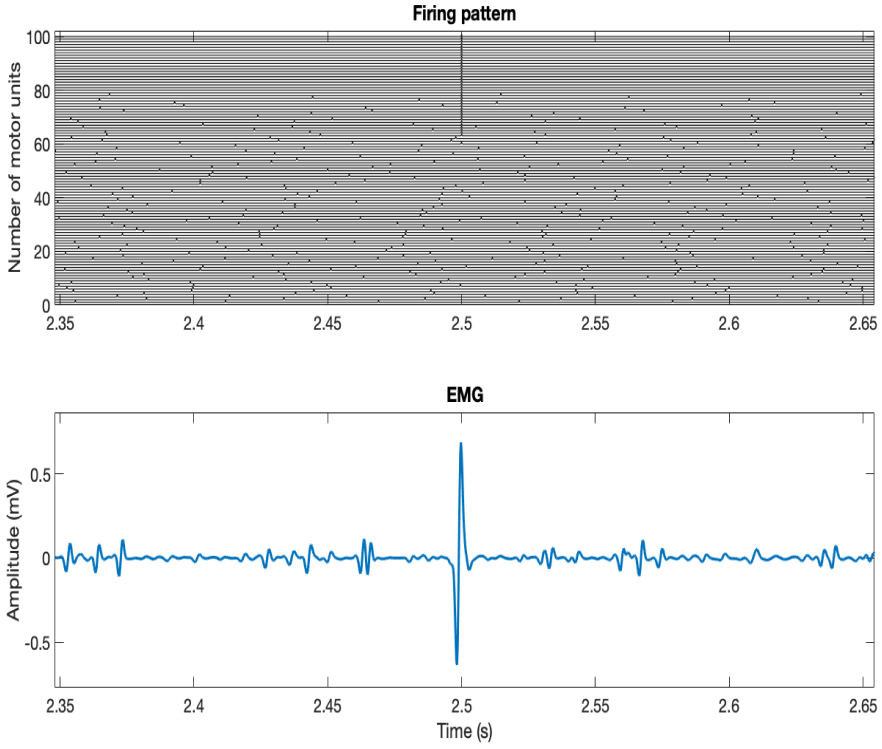

Figure 4.6: *Firing pattern and relative EMG obtained by a pool of 100 motor units: 40 MU are elicited by the stimulation, the others are recruited from voluntary contraction*

4.3.3 Morphological change of the M-wave

The difference in amplitude and width of the elicited M-wave, due to the refractoriness of motor units, was evaluated with several morphological parameters [35]:

- the peak-to-peak amplitude;
- the negative peak amplitude;
- the area of the negative peak;
- the half-area of the negative peak;
- the cross-correlation between different M-waves.

In the literature, it has been observed that the negative peak of the M-wave is more sensitive to changes in the shape of the signal (Fig. 4.7).

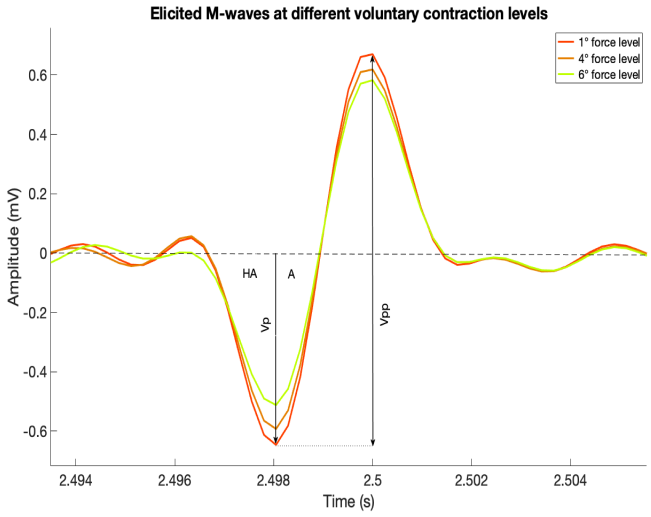

Figure 4.7: *Morphological parameters of the M-wave: Vpp represents the peak-to-peak amplitude, Vp is the negative peak amplitude, HA is the half-area of the negative peak, and A is the area of the negative peak.*

In-depth analysis has shown that the morphological parameters relative to the area weren't very indicative, so it was chosen to discard them since they were implicitly taken into account by the cross-correlation.
The parameters trend was analyzed at different levels of excitatory drive. Data were interpolated using a third-order polynomial curve. Three functions were tested to determine the point at which the MUs recruited by the central nervous system overlap with those excited by stimulation:

- *knee_pt* is a function that works by traversing along the curve, one bisection point at a time. It fits two lines, one to all the points on the left of the bisection and another to all the points on the right. The knee is determined to be at the bisection point that minimizes the sum of errors for both line fits [36].

- *kneed* implies the computation of the difference between the cumulative sum curve, normalized between 0 and 1, and the 45-degree intercept. The point where this difference reaches the maximum is valued to be the knee point. It is a function present in Python libraries [37].

- *knee_diff* involves the first-order derivative of the distribution of values. The point where the difference between two consecutive values of a parameter surpasses a certain threshold, defined as

$$t = \frac{max(x) - min(x)}{N} \tag{4.7}$$

  where N is the number of total values.

The best function to find the knee is the last: knee_diff. An example of finding the morphological change of the M wave using the knee_diff function is shown in the figure (Fig. 4.8).

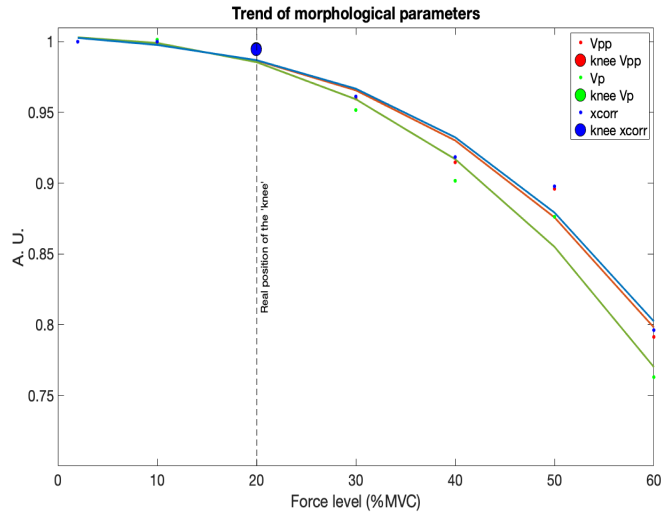

Figure 4.8: *Trend of morphological parameters over the force levels. Bigger circles represent the positions of the knee's distribution returned by the knee_diff function.*

4.3.4 Fatigue parameters analysis

An analysis of the spectral and amplitude parameters, in particular on the conduction velocity, was carried out on the results produced by the simulation.
During muscle contractions, some motor units are in a refractory period and do not contribute to the M wave. The motor units that do not contribute to the signal are likely the smallest ones that should be recruited by the electrical stimulus. Therefore, the conduction velocity of the M wave should increase as the level of force expressed becomes more intense.
Canonical fatigue parameters were calculated at different levels of simulated contraction, see Fig. 4.9. The Root mean squared value (RMS) and the average rectified value (ARV) describe the amplitude of the M wave, which reduces as the force level increases, showing a negative trend. Conduction velocity (CV), as well as the mean frequency (MNF) and the median frequency (MDF), are spectral factors related to the temporal support of the signal. CV was computed using the beamform method, see chapter 2.16. Since smaller motor units activate more slowly and may not contribute to the M-wave, it propagates faster. As a result, spectral parameters increase over the level of contraction.

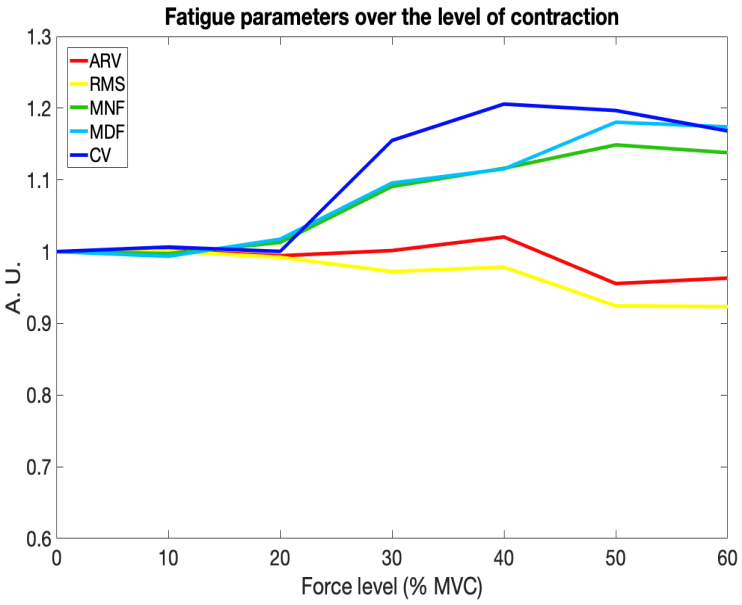

Figure 4.9: *Trend of fatigue parameters over the force levels.*

In conclusion, it can be stated that the hypotheses underlying the study are confirmed to a certain extent from the simulations. Furthermore, using the model of a pool of motor neurons it was possible to refine the aspects considered during the development of the experimental protocol.

4.4 Experimental protocol

The study involved 13 subjects (6 males and 7 females) who participated as volunteers. Each subject signed an informed consent document that outlined the purpose and activities of the study. The experimentation phase was conducted at *LISiN* (Laboratory for Engineering of the Neuromuscular System).
Each subject sat on the designated chair and placed their right hand on the measuring instrument with the palm facing upwards, the wrist stabilised in contact with the latex support and the thumb contacting the load cell. Before measurement, the subject was given brief training to ensure they understood the correct movement. They had to contract the muscle, pushing the thumb upwards, and performing an isometric contraction.
The experimental protocol is divided into two phases: in the first phase the subject is instrumented with the sensors and his MVC and SMC values (necessary to proceed with the second section) are estimated, while the second phase is characterized by the execution of the task. The whole experimental set-up is described in Fig. 4.10. The electrostimulator used is the *DS7A*, a current-driven stimulator (see Chapter 3.3.2) [38]. The EMG amplifier employed is the *EMG-16* [39].

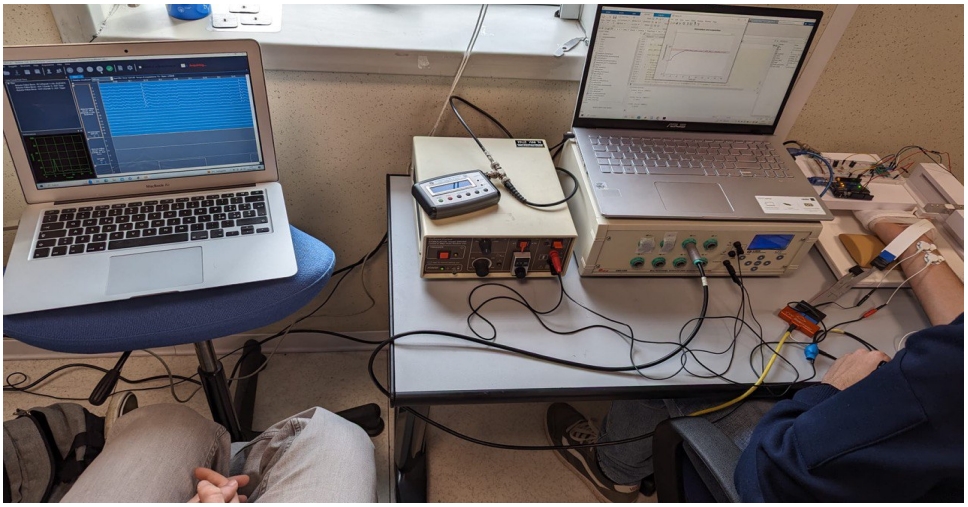

Figure 4.10: *Experimental set-up. The PC on the left is connected to the EMG amplifier and is used to visualize the EMG signals. In the middle, there are the electrical stimulator (on which the trigger input device is visible), the EMG amplifier, and another PC (on the EMG amplifier), used for the force feedback connected to the Arduino UNO board (placed on the measuring instrument). On the right is placed the measuring device. Also on the right it is possible to see the subject's hand placed on the measuring instrument while performing the exercises.*

Phase 1

In the first step, the subject has been asked to perform a maximal contraction for 10 s in order to estimate the MVC. This is necessary to establish the force levels as a percentage of MVC for the following phases of the experiment. The maximal contraction is repeated 3 times, with a rest period of 3 min between two contractions [40].
The acquisition electrodes were connected via cables to the EMG amplifier (Fig. 4.10). Before positioning the electrode array on the subject, it was necessary to clean the skin with the abrasive paste in correspondence with the target muscle. Two reference electrodes were positioned on the subject: respectively on the elbow, in correspondence with the olecranon bone, and on the shoulder, approximately above the acromion bone. Afterwards, using a dry electrode array, the correct orientation of the muscle fibres was found, with the help of visual feedback of EMG signals on the screen (Fig. 4.11).

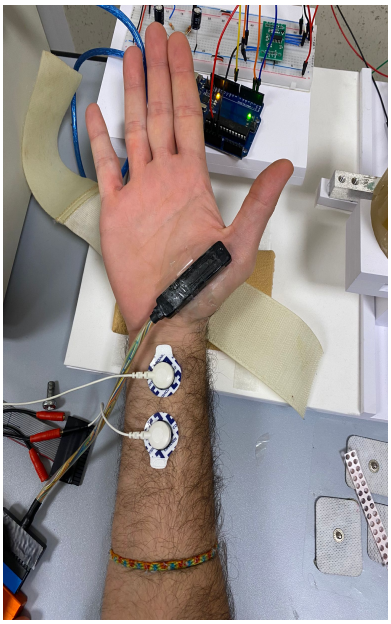

Figure 4.11: *Stimulating electrodes placed over the median nerve and a dry electrode array positioned over the abductor pollicis brevis to find the right fibres' orientation.*

Finally, the adhesive electrode array (inter-electrode distance of 5mm), previously prepared with double-sided tape and conductive paste, was placed on the target muscle.
Then, the localization of the median nerve was estimated [41]: in this site, the skin was cleaned again with the abrasive paste at the wrist, and two mobile stimulation

electrodes were used in bipolar mode, properly wet to reduce the skin-electrode impedance. Pulses of current (10 mA, 1 Hz) were delivered to the subject, and the electrodes were repeatedly moved to find the nerve. The optimal stimulation point was found when the thumb showed better mechanical and electrical feedback, assessed by watching the movement of the finger and the EMG feedback on the screen (visible thanks to the acquisition electrodes) after the arrival of the electrical impulse. When the stimulation points of the median nerve were found, adhesive electrodes were applied above.
The successive step was to estimate the SMC. Various pulses of increasing intensity were sent to the subject with a step of 2 mA starting from 8-10 mA up to 26 mA. For each value, 10 pulses are sent at a frequency of $1Hz$ and duration of 200 mus [42]. The data is subsequently processed in real-time to identify the SMC. The muscle response increases until it reaches a plateau: the minimum value after which the M-wave remains more or less stable corresponds to the SMC value. The SMC individuation was important to set the stimulation levels as a percentage of the SMC.

Phase 2

This part of the experimental protocol is important to determine the contraction level at which the M-wave changes morphology and decreases its amplitude: this means that the MUs recruited by the electrical stimulus overlap with those recruited by the CNS.
The subject was asked to perform exercises following visual force feedback on the screen: the feedback was shown by a line with an error range that varies depending on the force to be expressed, and the level of contraction to be performed. The subject had to maintain a constant voluntary contraction for a period of 15 s at certain force level, previously defined as a percentage of his MVC. Contractions were performed from 10% to 60% of MVC in 10% steps. After each force level, the subject rested for 30 s, during which the data of the exercise just performed was saved. During the contractions, electrical impulses of constant intensity, calculated as a percentage of the SMC at a frequency of 3 Hz, were sent to the subject.
To summarize, the stimulation levels considered were 50-60-70% of the SMC. The various exercises therefore consisted of stimulating the subject at a specific stimulation level, while he performed an isometric contraction at different contraction levels. Subsequently, everything was repeated for each stimulation level. Between one level of stimulation and another, the subject was allowed a recovery period of 3 min, needed for the complete restoration of the muscle [43].
Finally, the clean M-wave was detected, without voluntary contraction, but only by sending stimuli at a frequency of 1 Hz for 10 s. This last step was fundamental in order to obtain the differential M-wave between different force levels.

4.5 Signal processing

The processing of the acquired signals was carried out using Matlab software. Data was corrupted by motion artifacts, stimulation artifact and network interference noise. Thus, they were appropriately removed using software techniques.
As shown in Fig. 4.12a and in Fig. 4.12b, there are eight recording channels, each corresponding to an electrode on the array. The first channel is placed distally from the stimulation site, therefore it acquired a low-intensity signal, clearly separated from the stimulation artifact. On the contrary, the last recording channel is located proximal to the stimulation point and it displayed a greater response, partially overlapping with the artifact.

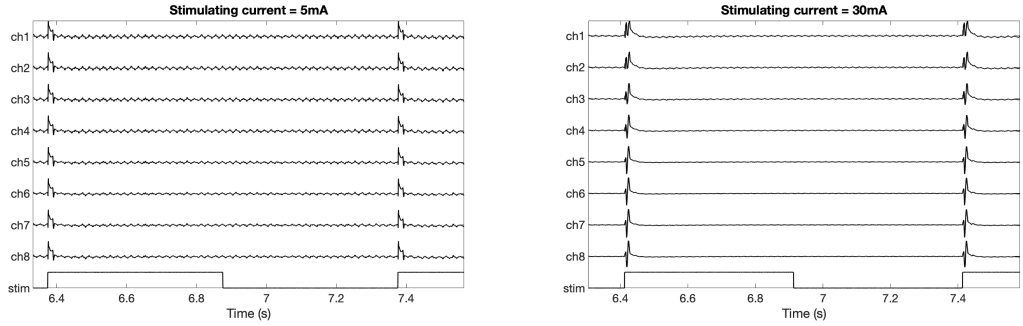

(a) *Stimulating current = 5mA* **(b)** *Stimulatin current = 30mA*

Figure 4.12: *Recordings at different level of stimulation: (a) shows the signals recorded when the stimulating current was equal to 5 mA, (b) represents the signal acquired from the same subject when the current of stimulation was 30 mA.*

Noise interference at 50 Hz can be observed from the recorded signals (Fig. 4.13a). To get rid of this noise, a recursive filter was applied to the data. The recursive filter attenuates the noise with a factor of 100 and a bandwidth of 2 Hz centered on the 50Hz frequency.
Additionally, motion artifacts resulting from thumb movement due to electrical stimulation, were removed using a high-pass Chebyshev filter, with a cut-off frequency set to 15 Hz. To ensure that signals weren't corrupted by high-frequency disturbances, a low-pass filter was applied to the data, with a cut-off frequency set to 400 Hz.
As a result, the power spectral density (PSD) of the elaborated data lies within the frequency band of the EMG signal, as it is demonstrated in Fig. 4.13b.
The PSD was calculated according to the Welch method (see paragraph 2.3.2), by using a rectangular window of the same length in samples as the recorded signal.

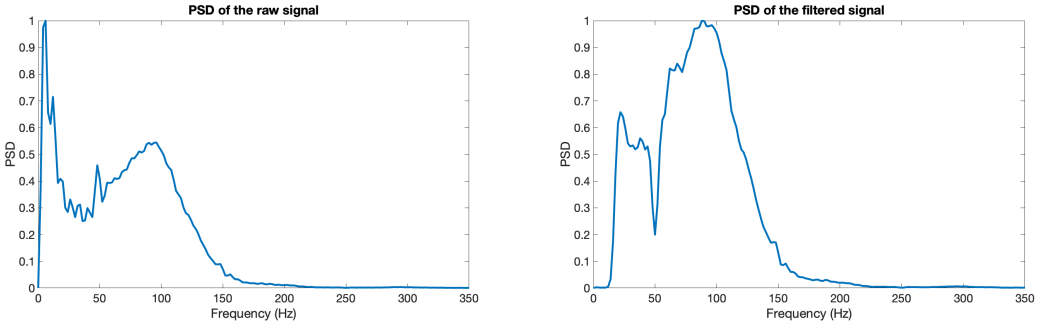

(a) *PSD of the raw signal* **(b)** *PSD of the filtered signal*

Figure 4.13: *PSD of the signal at different steps of the processing: a) represents the PSD of the raw data; b) shows the PSD obtained after the application of the recursive filter and the low-pass filter.*

The noise-free signals were averaged over the number of stimuli delivered to the subject, to make results more repeatable. Fig. 4.14a represents the recording epochs and Fig. 4.14b shows the resulting averaged signal.

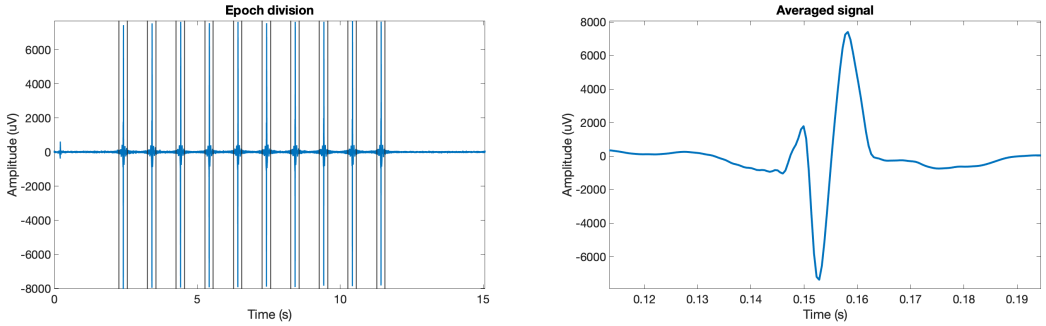

(a) *Different epochs* **(b)** *Averaged signal*

Figure 4.14: *Averaging performed over different recordings epochs. 200 samples were taken before and after the on-set stimulation, in order to highlight the M wave a). The resulting signal is still affected by the stimulus artifact, but the signal-to-noise ratio (SNR) is higher b).*

The averaging between epochs emphasizes the deterministic traits of a signal and attenuates the influence of stochastic processes [44]. The stimulation artifact is a non-propagating noise that occurs in samples that follow the stimulation on-set (see paragraph 3.4). Its removal was performed with the adaptive blanking

technique (Fig. 4.15). The number of samples to be deleted, which is defined after the computation of the mean frequency of the signal, was chosen based on the data recorded during the lowest stimulation level, since the acquired response was mainly affected by the stimulus artifact.

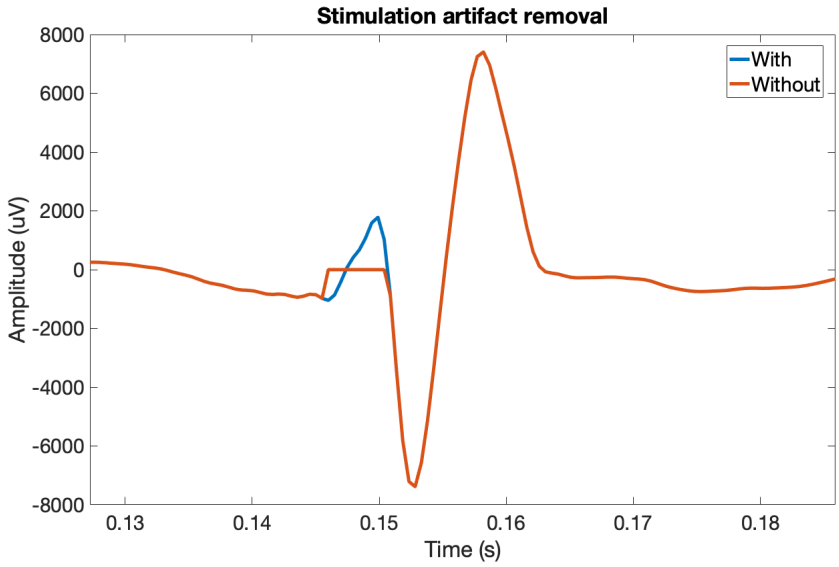

Figure 4.15: *Stimulus artifact removal with the adaptive blanking technique. The artifact appears in the first 10 samples after the stimulation on set.*

Signal processing was performed for both the first part of the experiment and the second, as noises affected the recordings for the entire duration of the experiment.

Chapter 5

Results

For each subject, it was necessary to calculate the maximum voluntary contraction (MVC) and the supra-maximal stimulation current (SMC).

5.1 Supramaximal stimulation

The different levels of current delivered to the subject resulted in different responses from the muscle. The SMC was defined as the current above which there was no significant increase in EMG amplitude [45]. Fig. 5.1a depicts the M waves elicited by different levels of stimulation for the first subject tested, while Fig. 5.1b shows the trend of the amplitude of the EMG as the stimulation current varies. The estimate of the SMC was made by processing the data in real-time, during the execution of the experimental protocol.

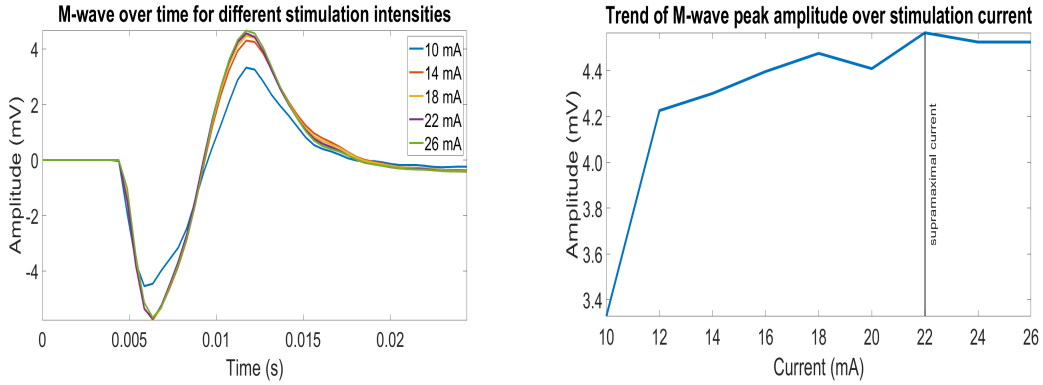

(a) *Different epochs for certain stimulation levels* **(b)** *Trend of M-wave amplitude*

Figure 5.1: *Estimation of supramaximal current.*

The average value of SMC computed over all of the subjects is equal to 20.09 mA, with a standard deviation of 2.02 mA. The result obtained is consistent with the findings reported in the literature [46].

5.2 Task's performance (single-case)

In the second part of the experimental protocol, the subject had to perform six isometric contractions for every level of electrical stimulation. During the contractions, current pulses at three different intensities were delivered at a frequency of 3 Hz. The results presented in that section refer to a single subject. The figures 5.2a, 5.2b, 5.2c show the 8 channels of the EMG signal recorded in the monopolar detection.
Note the overlapping of the M-wave (resulting from larger MUs recruited by the electrical stimulation) on the background EMG (resulting from smaller MUs recruited by the voluntary contraction).
The best channel for each subject was chosen and the averaging technique was applied: the 15 central M waves were then realigned and averaged to see how the amplitude and the morphological parameters changed as the contraction and the stimulation varied [47]. The following three figures on the left show the trends of the M wave over time as the contraction level varies for the three different stimulation levels.
On the right, figures show how the negative peak indicator varies. The negative peak indicator for this subject is the best indicator for locating the knee. The position of the knee (where the two pools of MUs overlap) is estimated with the function *knee_diff* (explained in section 4.5) and is highlighted with a blue circle and two dotted vertical lines. There is no overlap yet at the blue circle, while at the next one, it has already occurred, so the precise knee's location is found between the two dotted lines. Note that the maximum amplitude at 70% SMC is larger than that at 60% SMC and the amplitude at 60% SMC is larger than that at 50% SMC.
For this subject, the M-wave shape is very similar to the M-wave shape obtained with the simulation model.
As shown in the figures 5.4, it is possible to note that the spectral parameters (average frequency and median frequency) tend to decrease as the contraction increases for all stimulation levels, while the amplitude parameters (root mean square and average rectified value) present greater variability: the RMS tends to increase, while the ARV tends to remain relatively constant as the contraction levels increase. The CV, on the other hand, has an increasing trend for the first levels of contraction, while decreasing for the last ones.

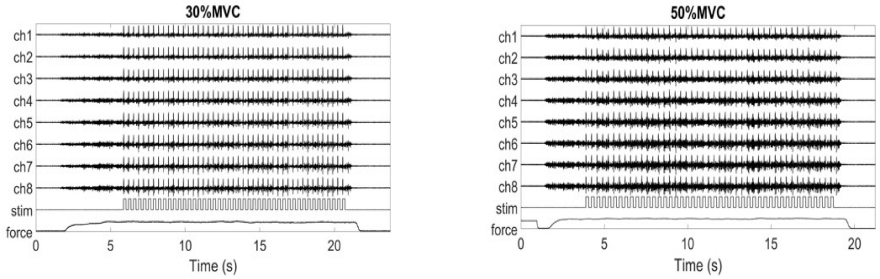

(a) *The figure shows two different levels of contraction (30% MVC and 50% MVC), with stimulation at 50% SMC*

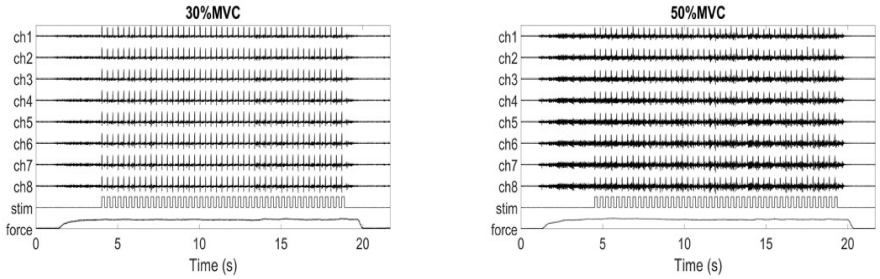

(b) *The figure shows two different levels of contraction (30% MVC and 50% MVC), with stimulation at 60% SMC*

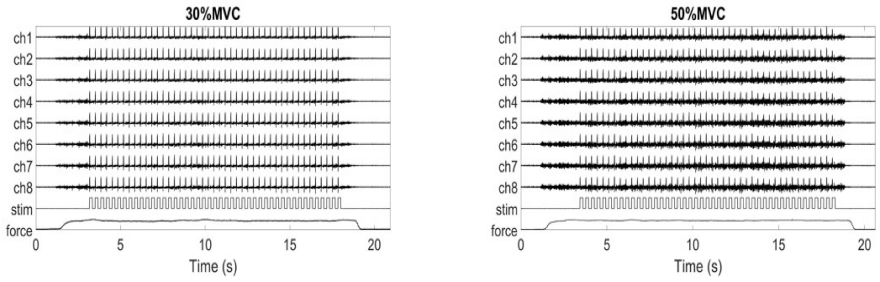

(c) *The figure shows two different levels of contraction (30% MVC and 50% MVC), with stimulation at 70% SMC*

Figure 5.2: *The EMG channels for the three different stimulation levels. Only two levels of contraction are represented: 30% and 50% of the MVC. The last two rows of each figure: stim and force, respectively represent the trigger signal of electrical stimulation and the force signal.*

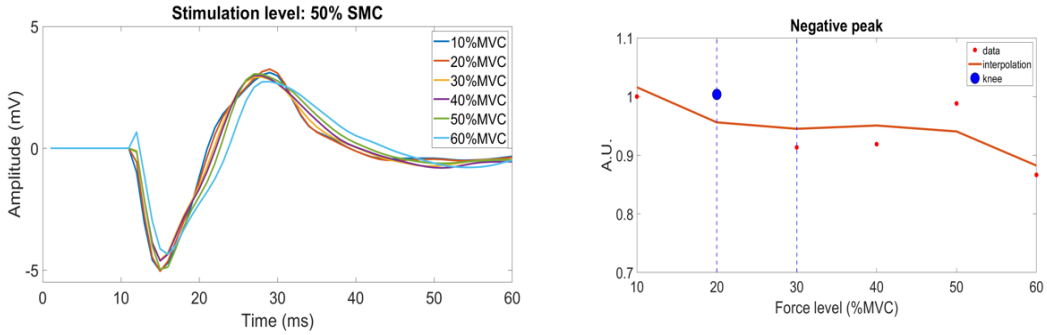

(a) *Trend of M-wave amplitude over contraction levels and the knee position when the stimulation is at 50% SMC.*

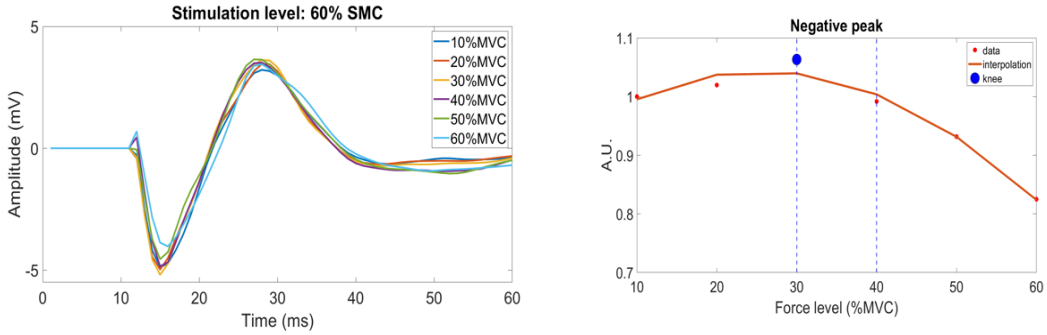

(b) *Trend of M-wave amplitude over contraction levels and the knee position when the stimulation is at 60% SMC.*

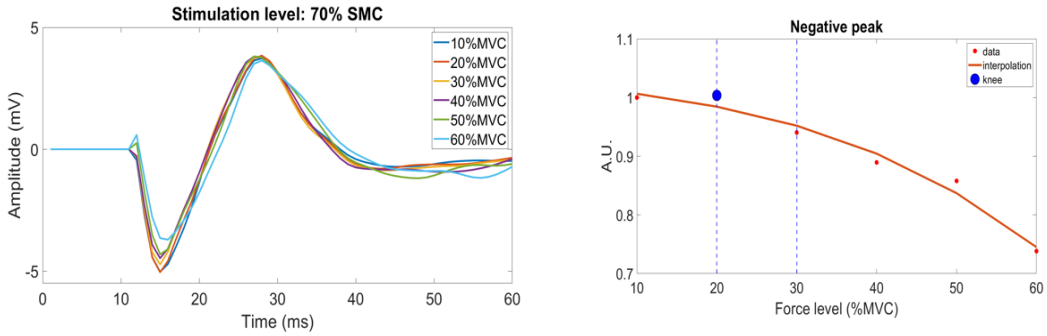

(c) *Trend of M-wave amplitude over contraction levels and the knee position when the stimulation is at 70% SMC.*

Figure 5.3: *On the left there are the M waves elicited at three different stimulations over different contractions and on the right the trends of the negative peak at the corresponding stimulation level are represented. The position of the knee is highlighted.*

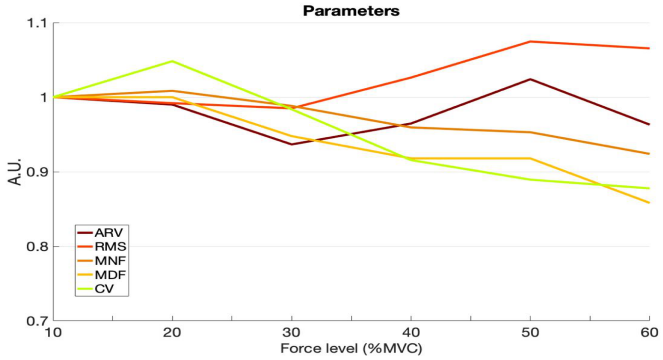

(a) *Conduction velocity, amplitude and spectral parameters estimated for a stimulation level of 50% SMC.*

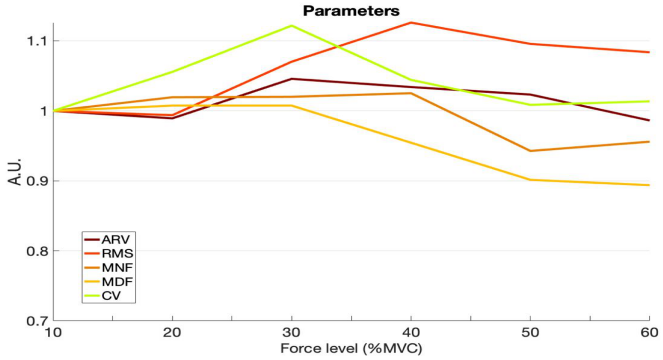

(b) *Conduction velocity, amplitude and spectral parameters estimated for a stimulation level of 60% SMC.*

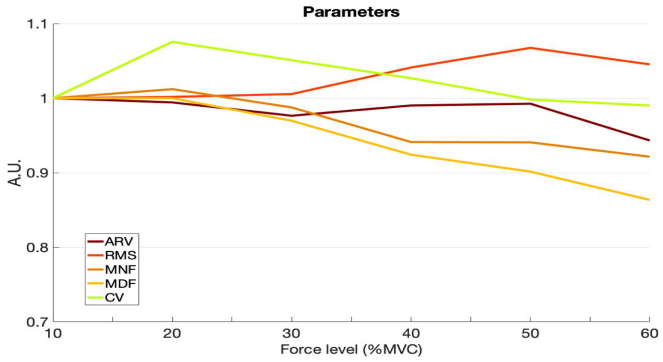

(c) *Conduction velocity, amplitude and spectral parameters estimated for a stimulation level of 70% SMC.*

Figure 5.4: *Conduction velocity, amplitude parameters (ARV and RMS) and spectral parameters (MNF, MDF) estimated for the different stimulation levels.*

Finally in figure 5.5 the differential estimations of the M-waves between two force levels are shown.

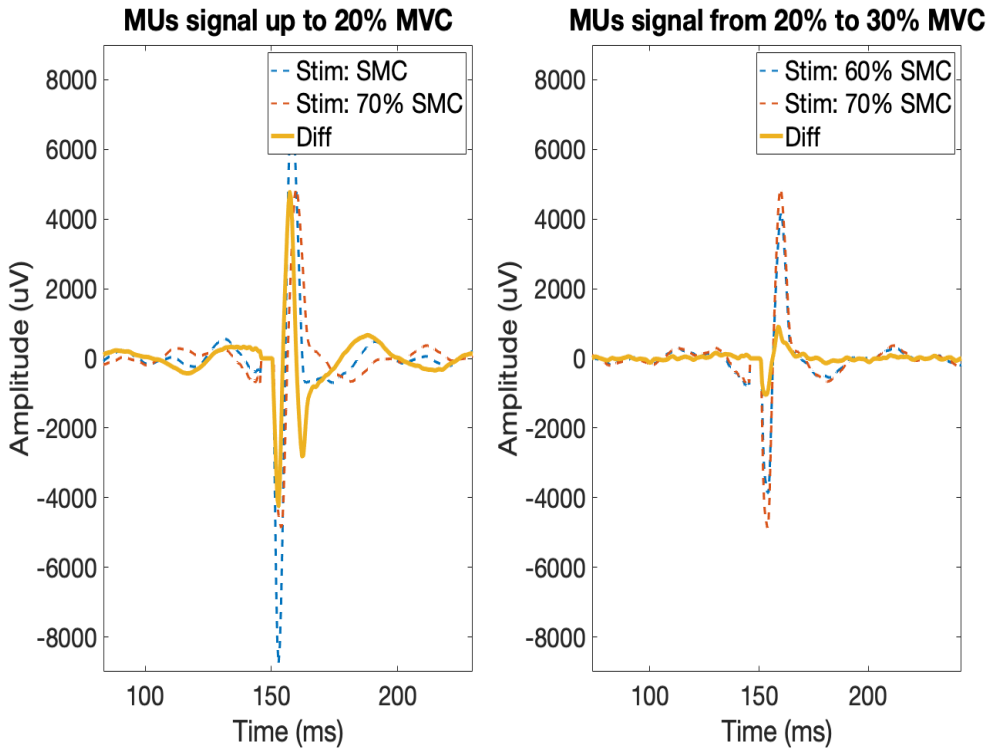

Figure 5.5: *Differential M-waves are represented in yellow and the original monopolar signals are represented in dotted lines.*

For this specific subject, on the left side of the figure it is represented in yellow the signal of the motor units (MUs) that are activated up to 20% of maximum voluntary contraction (MVC). The differential M-wave is estimated as the difference between the M-waves elicited during a supramaximal current stimulation and at 70% SMC (they are shown with dotted lines in the figure).
On the right side of the figure, the signal of the MUs activated from 20 to 30% MVC is shown. It is estimated as the difference between the M-waves at 60% SMC and 70% SMC (shown with dotted lines in the figure).

5.3 Task's performance (multi-case)

The processed M-wave signals for all the subjects (13 subjects in total, 7 females and 6 males with a mean age of 24.6 years) who took part in the experiment are displayed below (Fig. 5.6).

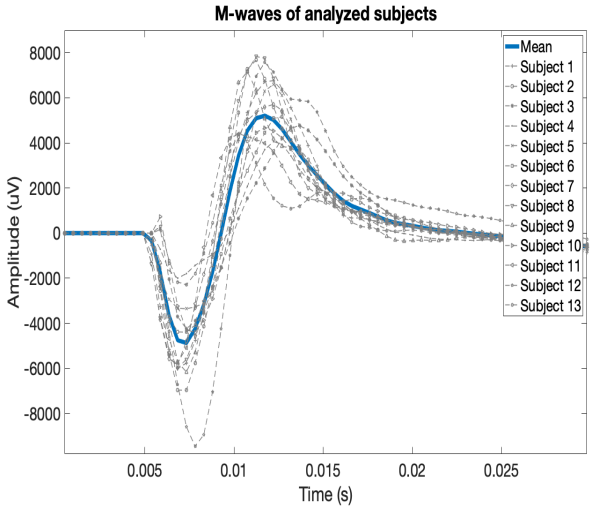

Figure 5.6: *Superimposition of the different M-waves calculated for each participant in the study. The figure refers to the results obtained when the electrical stimulation was set equal to 70% SMC and the level of voluntary contraction equal to 10% MVC. The curve in blue represents the mean signal.*

The dynamics of the signal and the temporal support are approximately the same for all subjects, consequently, it was possible to obtain an average wave with a well-defined morphology.
The average M wave was calculated for all stimulation levels and all contraction levels, as shown in Fig. 5.7.

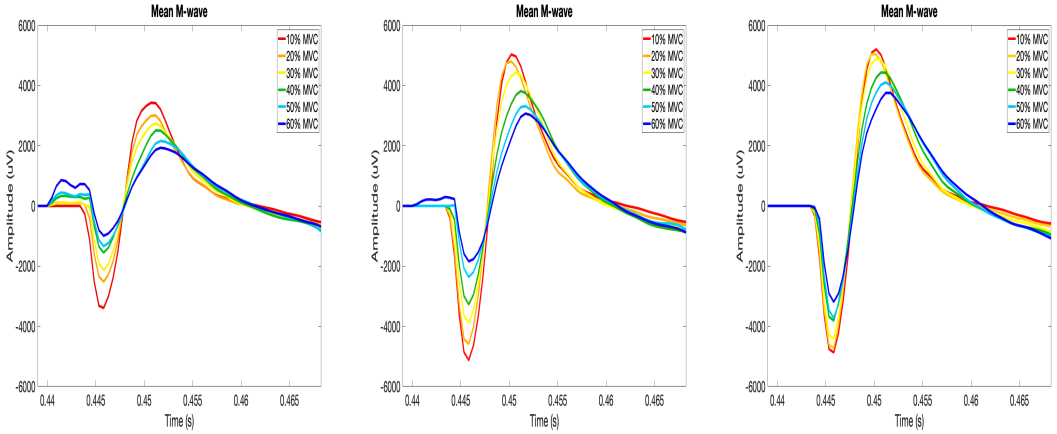

(a) *50% SMC* **(b)** *60% SMC* **(c)** *70% SMC*

Figure 5.7: *Mean M-wave evaluated over different force levels.*

The knee position was found for every subject. Results are described in Fig.5.8a and in Fig.5.8b.

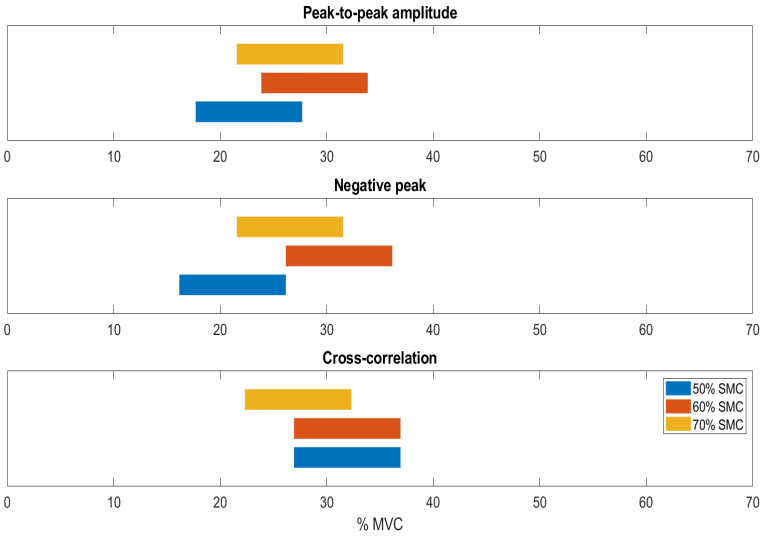

(a) *Interval of the knee position for all the subjects.*

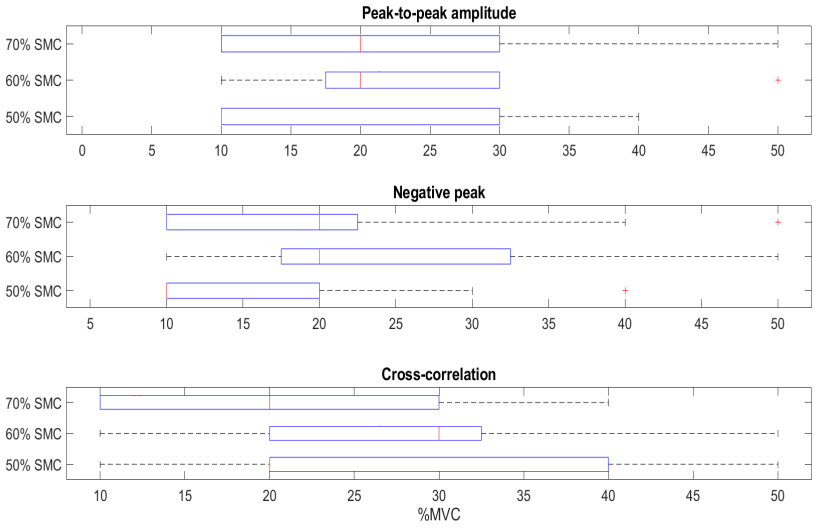

(b) *Boxplot of knee position*

Figure 5.8: *Knee position over force level. a) shows the mean interval where the knee point was found for different morphological parameters. The box plot figures the variability in knee position performed for all subjects.*

The differential M-wave, obtained by the difference between the signals resulting from two different levels of stimulation (70% SMC and 60% SMC), is represented in Fig. 5.9.

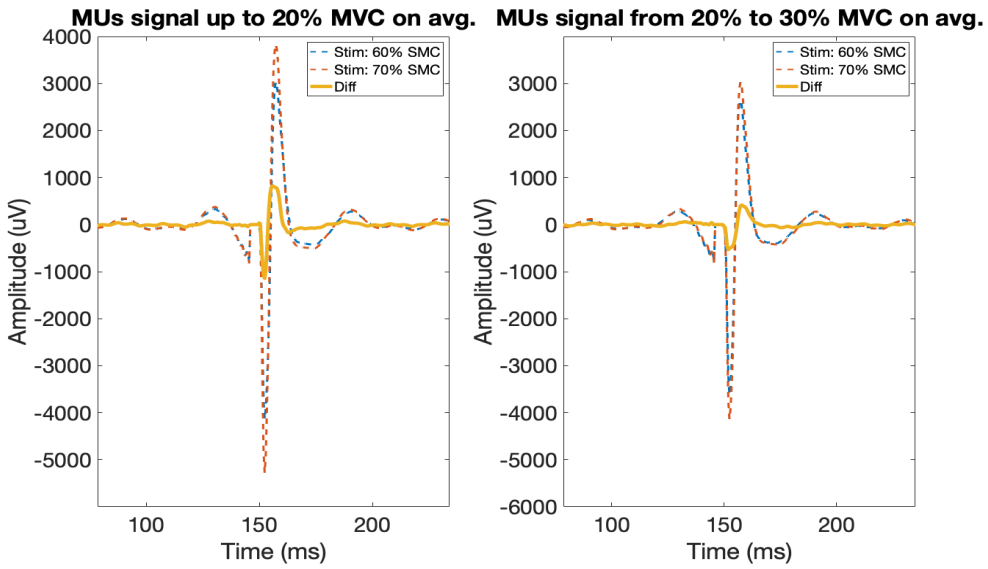

Figure 5.9: *In the figure, the differential M-waves is shown. The one on the right is computed by subtracting the M-wave at 60% SMC to the M-wave obtained at 70% SMC. The result is averaged over all the subjects analyzed, since the knee point for these levels of electrical stimulation was found between 20% MVC and 30% MVC, the signal in yellow should be indicative of the MUs activating between these levels of contractions. The other image represents the difference between the signal recorded when the stimulation was supramaximal and the signal obtained at 70% SMC. It is indicative of MUs that activate when the force is at 20% MVC.*

The other experimental results are summarized in the box plots in Appendix A. The red line represents the trend average values of the different parameters.

Chapter 6

Discussion of the results and conclusion

The results of the experimental phase, presented in Chapter 5, are analyzed in this last chapter. The results obtained from the simulations, presented in the section 4.3.2 are also discussed. Moreover, the problems during the experimental phase are highlighted in order to offer ideas to improve future experiments.

6.1 Analysis of the simulation results

In Fig. 4.9 the trend of the fatigue parameters over the contraction level is shown. In particular, as the voluntary contraction increases, RMS and ARV tend to remain constant up to 40% MVC, after which a slight decrease is noted. This is expected because the area under the M-wave is reduced for the highest contraction levels (50 and 60% MVC). The other parameters (MNF, MDF and CV) have a more distinct trend: they have a clearer increase after 20% MVC. MNF and MDF increase because of the reduction of temporal support, as shown in Fig. 4.7. CV instead increases as the contraction level rises and more MUs are recruited by the central nervous system. Due to this, the stimulus only recruits the larger motor units that are not in the refractory period and have a higher conduction velocity.

6.2 Analysis of the experimental results

The plot in Fig. 5.6 refers to a stimulation level of 70% and a contraction level of 10%. It shows in blue the averaged M-wave and in grey the M-wave for all the single subjects for the same stimulation and contraction level. The averaged M-waves for all contraction levels and all stimulation levels are shown in Fig. 5.7. It is evident

that the peak-to-peak amplitude of the M-wave decreases as the contraction level increases, and increases as the stimulation level increases. These two outcomes align with the simulation results. However, it is important to note that the M-waves widen as the contraction increases. From a more careful analysis, it is possible to see that the M-wave at 20% MVC tends to be narrower than that at 10%, and then widens. This result does not align with what is observed in the simulations (a possible explanation is described below in the second point of the section 6.3).
Fig. 5.8a shows the mean position of the knee averaged for the different subjects. The average trend is calculated for all the selected indicators to determine the knee position. The knee position should be within the indicated ranges for each stimulation level: the left limit is the point at which the overlap of the MUs has yet to occur, while the right limit indicates that it has already occurred. The knee is therefore in that range. The finding trends align with the simulation results for 60 and 70% SMC across all indicators, but the situation deteriorates at 50% SMC. In the latter case, the range was expected towards higher MVC values, i.e. between 35/40 and 45/50% MVC. The discrepancy in these experimental results compared to the simulations is likely attributed to sub-optimal signal processing, as the M-wave is obscured by the background EMG for many participants at the 50% SMC.
It is possible to make similar observations for Fig. 5.8b in which the box plots are displayed for each indicator and for the different stimulation levels. It is important to note the wide dispersion of the data, which is likely due to the difficulty of precisely locating the knee (as explained in the first point of the section 6.3).
In Fig. 5.5 it is important to note that the signal of MUs of the left image has a greater amplitude than the signal of the right image. The reason may be attributed to the greater number of motor units that are activated up to 20% MVC compared to the number of motor units recruited for contractions ranging from 20 to 30% MVC.

6.3 Critical issues and future developments

Some significant critical issues have been encountered during the experimental phase and data processing. They are summarised in the following points.

- **Issues in finding the knee**

  The identification of the knee is strongly influenced not only by the spatial recruitment but also by the temporal recruitment of the MUs. The latter is correlated to the firing frequency of each MU and therefore also to its refractory period that only lasts a few milliseconds. Moreover, the last MUs

recruited by CNS have a few Hz firing rate. These two factors complicate the identification of the knee in both simulations and experimental settings. As shown in Fig. 6.1, the probability of MUs recruited by the CNS during a refractory period increases as their firing frequency increases and therefore the level of contraction increases. For low contraction levels, thus, the overlap of the MUs could not be detected correctly, as the last MUs recruited by the CNS by firing slowly are also recruited by the stimulus. For these reasons, the obtained results may overestimate the actual position of the knee. However, by averaging over 20 different stimuli, these problems did not have a significant impact. These issues, which were slightly noticeable during simulations, become more pronounced during the experimental phase due to less control over the various parameters.

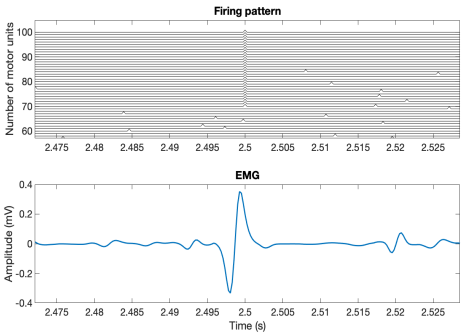

(a) *Firing pattern when a few MUs are in a refractory period*

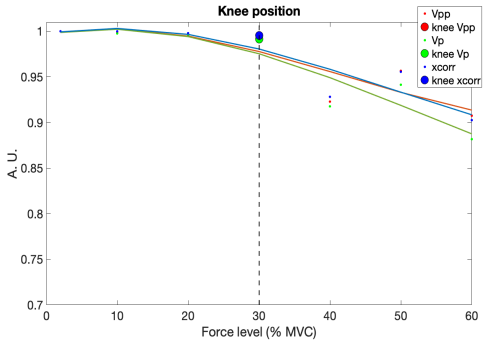

(b) *Position of the knee*

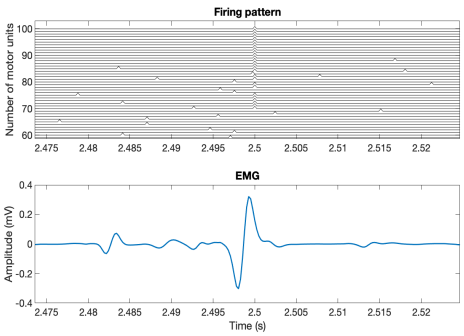

(c) *Firing pattern when more MUs are in a refractory period*

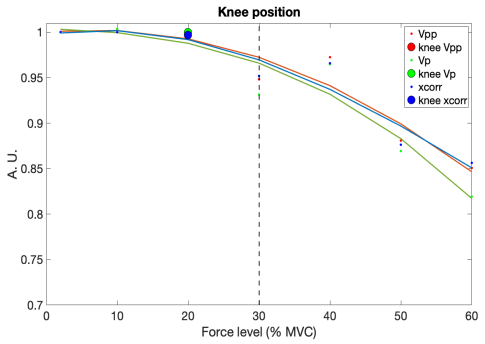

(d) *Position of the knee*

Figure 6.1: *Simulation results: different outcomes of the position of the knee when stimulation and force level are the same.*

- **Experimental outcomes in contrast with simulation results**

  In order to explain the M-wave widening, in contrast with the simulation results, the fatigue parameters over contraction level are analyzed as shown in Fig. 5.4. These parameters refer to a single subject but are indicative of all subjects. Note that the ARV and RMS values tend to remain constant and increase slightly, respectively, while in the simulations they show a slightly decreasing trend. In this case, the increase in the M-wave's bulging may be compensating for the reduction in peak-to-peak amplitude, resulting in a slight increase in these parameters. The spectral parameters both tend to decrease, in contrast to the findings of the simulations. The CV exhibits a distinctive trend. Initially, for low force levels, the CV increases. However, after reaching 20-30% MVC, it begins to decrease. Also this finding stands in contrast to the outcomes obtained in the simulations.
  The trends in these parameters may be attributed to muscle fatigue during task execution, as evidenced by the fatigue plots over time in Fig. 6.2

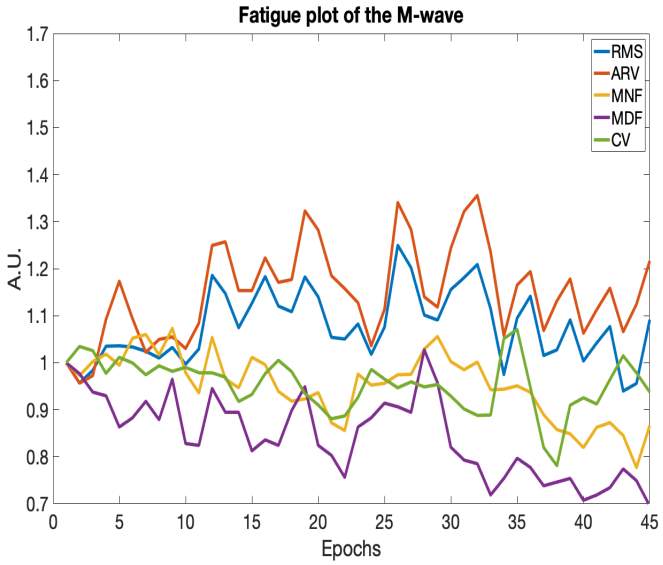

Figure 6.2: *Fatigue plot of the M-wave evaluated when the stimulation was equal to 70% SMC and contraction level to 50% MVC. RMS, ARV, MNF, MDF and CV trend over different epochs.*

Muscle fatigue may have caused the difference between the simulation and experimental results, as fatigue tends to affect the amplitude, spectral parameters and CV, in the opposite way to what is expected in the experiment. It's crucial to note that the trend of these parameters is calculated based on the samples of the M-wave, indicating fatigue in the larger MUs. These

MUs are stimulated at 3Hz for 15s, and it is surprising that they fatigue at such a low frequency. Conversely, smaller MUs exhibit signs of fatigue for the higher contractions as shown in Fig. 6.3, which depicts the fatigue plot of the background EMG. When the smaller motor units become fatigued, they create an acidic environment in their surroundings.

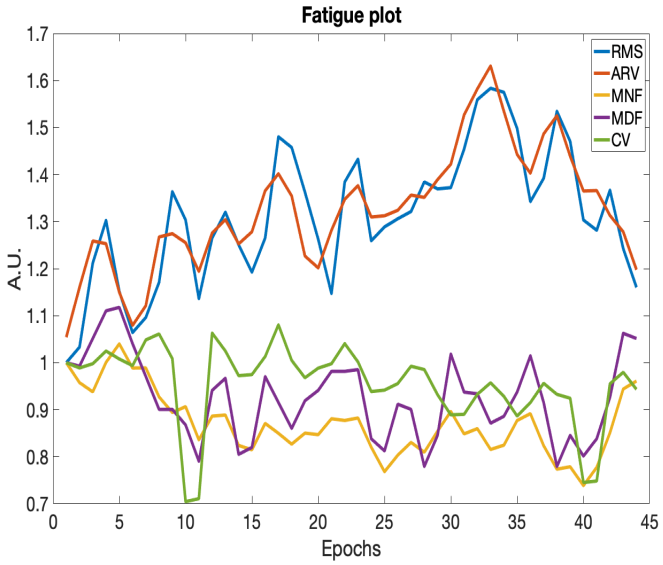

Figure 6.3: *Fatigue plot of background EMG evaluated when the stimulation was equal to 70% SMC and contraction level to 50% MVC. RMS, ARV, MNF, MDF and CV trend over different epochs.*

Their fatigue and resulting acidification may induce fatigue in the larger MUs responsible for generating the M-wave, potentially contributing to its observed widening. Furthermore, as shown in Fig. 5.4, fatigue seems to occur for the highest contraction levels, as the CV initially increases and then when fatigue occurs it decreases.

- **Experimental problems in CV estimation**

The conduction velocity estimation may have been affected by errors because, for some subjects, sweating occurred under the acquisition electrodes during electrical stimulation. This made it uncertain whether the acquisition electrode array remained in position, as it likely underwent small movements that misaligned it from its initial position, parallel to the muscle fibres. The misalignment between fibres and electrode array could be the cause of any errors.

Future developments

To address the issues mentioned above, it is important to pay close attention during the experimental phase.
One common approach used to reduce fatigue during the protocol is to make the subject perform different voluntary exercises randomly [48]. This may help minimize the effects of muscle fatigue. To determine the exact position at which the M wave changes in shape, it is recommended to maintain constant stimulation at two levels (for example 60% SMC and 70% SMC) and gradually increase the voluntary contraction in smaller increments.
In conclusion, this work has potential applications in rehabilitation and diagnostics, but is primarily rooted in the research field. While similar studies have been conducted on motor units analysis [49], this approach is innovative compared to the existing literature.

Appendix A

Experimental results

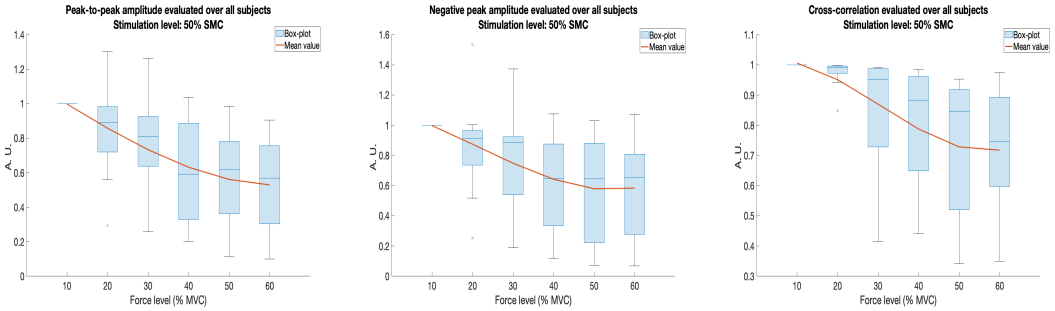

(a) *Peak-to-peak amplitude* **(b)** *Negative peak amplitude* **(c)** *Cross-correlation*

Figure A.1: *Trend of morphological parameters when stimulation is 50% SMC.*

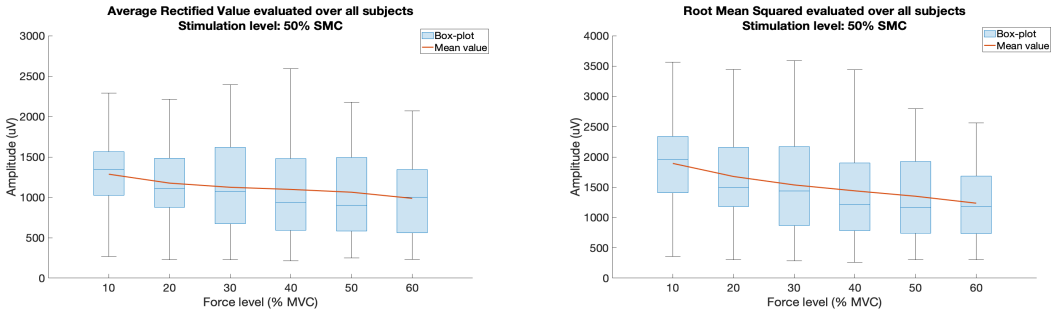

(a) *ARV* **(b)** *RMS*

Figure A.2: *Trend of ARV and RMS when stimulation is 50% SMC.*

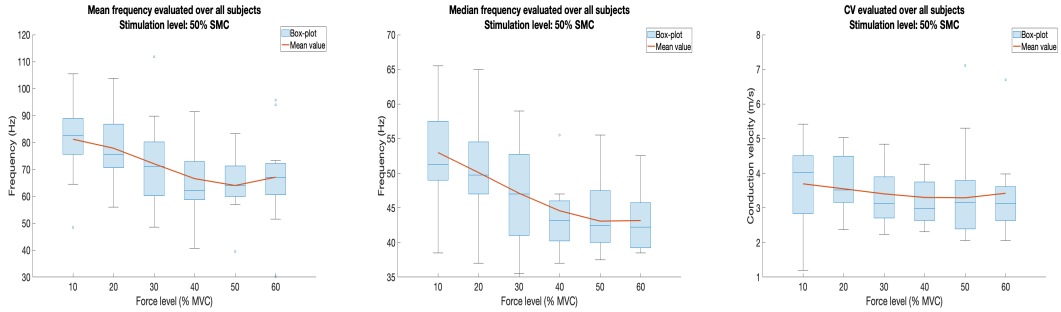

(a) *Mean Frequency* **(b)** *Median Frequency* **(c)** *Conduction velocity*

Figure A.3: *Trend of spectral parameters when stimulation is 50% SMC.*

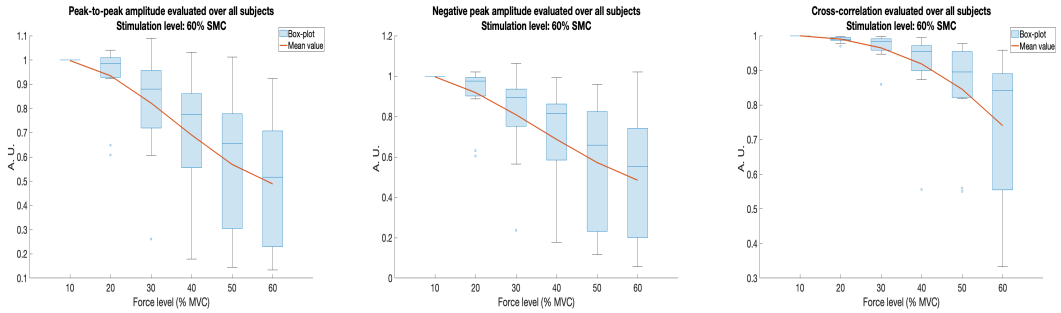

(a) *Peak-to-peak amplitude* **(b)** *Negative peak amplitude* **(c)** *Cross-correlation*

Figure A.4: *Trend of morphological parameters when stimulation is 60% SMC.*

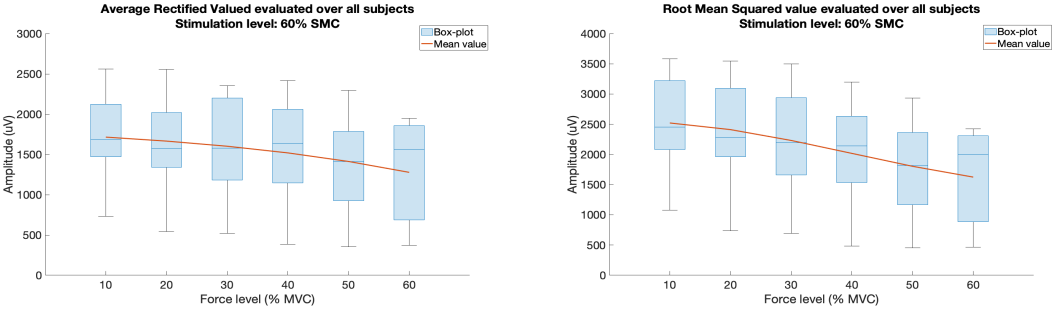

(a) *ARV* **(b)** *RMS*

Figure A.5: *Trend of ARV and RMS when stimulation is 60% SMC.*

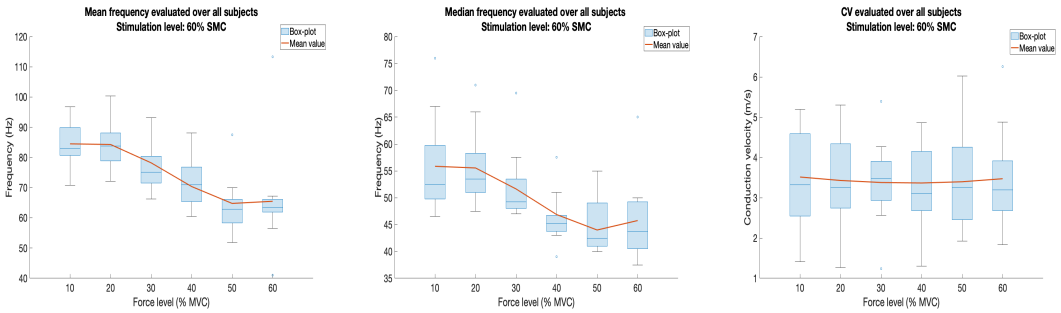

(a) *Mean Frequency* **(b)** *Median Frequency* **(c)** *Conduction velocity*

Figure A.6: *Trend of spectral parameters when stimulation is 60% SMC.*

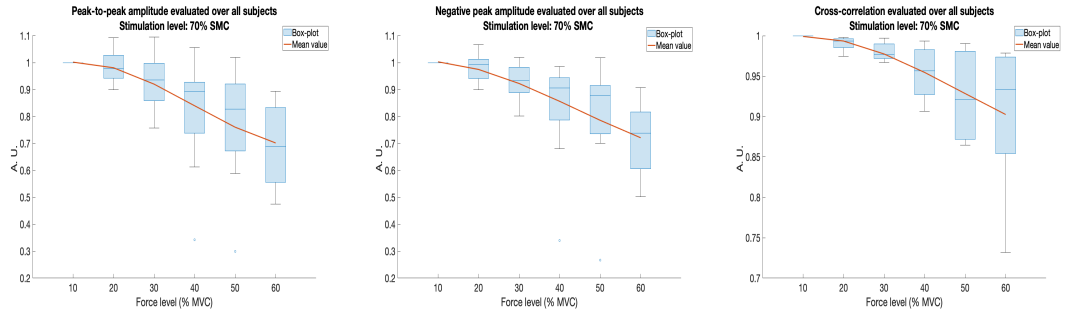

(a) *Peak-to-peak amplitude* **(b)** *Negative peak amplitude* **(c)** *Cross-correlation*

Figure A.7: *Trend of morphological parameters when stimulation is 70% SMC.*

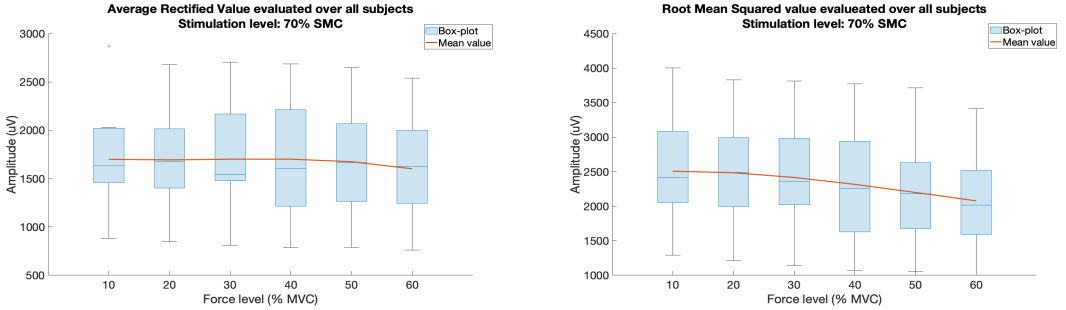

(a) *ARV* **(b)** *RMS*

Figure A.8: *Trend of ARV and RMS when stimulation is 70% SMC.*

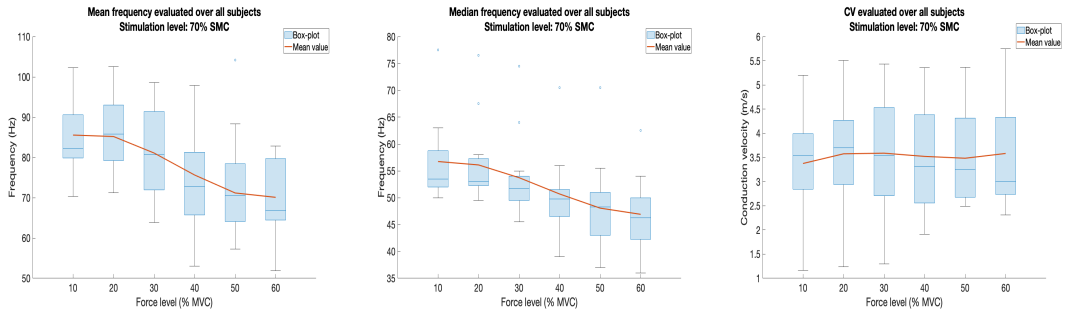

(a) *Mean Frequency* **(b)** *Median Frequency* **(c)** *Conduction velocity*

Figure A.9: *Trend of spectral parameters when stimulation is 70% SMC.*

Bibliography

[1] L. Mesin. *Neuromuscular System Engineering*. Torrazza Piemonte: IL MIO LIBRO, 2019 (cit. on pp. 1, 3, 6, 23, 36).

[2] Huxley A. F. Hodgkin A. L. «A quantitative description of membrane current and its application to conduction and excitation in nerve». In: *J. of Physiol.* 117 (1952), pp. 500–544 (cit. on p. 4).

[3] C. L. Stanfield. *Principles of Human Physiology - VI Edition*. University of South Alabama: Pearson Education, 2017 (cit. on pp. 6, 9).

[4] Renaud J.M. Mainwood G.W. «The effect of acid-base balance on fatigue of skeletal muscle». In: *Can J Physiol Pharmacol* 63 (1985), pp. 403–416 (cit. on p. 11).

[5] Purves D. et al. *Neuroscience. 2nd edition.* Sinauer Associates: Sunderland, 2001 (cit. on p. 11).

[6] Carpenter D.O. Hennemann E. Somjean G. «Functional significance of cell size in spinal motorneurons». In: *J Neurophysiol* 28 (1965), pp. 560–580 (cit. on pp. 12, 39).

[7] John G.Webster. *Medical instrumentation: application and design, fourth edition*. Hoboken, New York: John Wiley and Sons, 2009 (cit. on pp. 17, 20, 22).

[8] Marco Knaflitz. *Bioingegneria elettronica e sicurezza*. Torino: Levrotto and Bella, 2018 (cit. on p. 22).

[9] Robert I. Magnusson Lars H. Lindstrom. «Interpretation of Myoelectric Power Spectra: A Model and Its Applications». In: *Proceedings of the IEEE* 65 (1977), pp. 1–10 (cit. on p. 26).

[10] L. Mesin. *Introduction to biomedical signal processing*. Torrazza Piemonte: IL MIO LIBRO, 2017 (cit. on p. 26).

[11] R. Merletti D. Farina. «Methods for estimating muscle fibre conduction velocity from surface electromyographic signals». In: *Medical and Biological Engineering Computing* 42 (2004), pp. 432–445 (cit. on p. 28).

[12] Nussbaum El. et al. «Neuromuscular Electrical Stimulation for Treatment of Muscle Impairment: Critical Review and Recommendations for Clinical Practice». In: *Physiother Can* 69 (2017), pp. 1–76 (cit. on p. 29).

[13] Ingersoll C. Palmieri R. and Hoffmann M. «The Hoffmann Reflex: Methodologic Considerations and Applications for Use in Sports Medicine and Athletic Training Research». In: *Journal of Athletic Training* 39 (2004), pp. 268–277 (cit. on p. 30).

[14] Pozzo M. Farina D. Bianchetti A. and Merletti R. «M-wave properties during progressive motor unit activation by transcutaneous stimulation». In: *Journal of Applied Physiology* 97 (2004), pp. 545–555 (cit. on p. 31).

[15] Dean J. Bickel S. Gregory G. «Motor unit recruitment during neuromuscular electrical stimulation: a critical appraisal». In: *European Journal of Applied Physiology* 111 (2011), pp. 2399–2407 (cit. on p. 32).

[16] Orizio C. et al Gobbo M. Maffiuletti N.A. «Muscle motor point identification is essential for optimizing neuromuscular electrical stimulation use». In: *J NeuroEngineering Rehabil* 11 (2014) (cit. on p. 32).

[17] Merletti R. Knaflitz M. «Suppressionof Simulation Artifacts from Myoelectric-Evoked Potential Recordings». In: *IEEE Transaction on Biomedical Engineering* 35 (1988), pp. 758–763 (cit. on p. 33).

[18] Delgado J. M. R. Del Pozo F. «Hybrid stimulator for chronic experiments». In: *IEEE Transaction on Biomedical Engineering* 25 (1978), pp. 92–94 (cit. on p. 35).

[19] Merletti R. Farina D. Pozzo M. «Stimulation artifact in surface EMG signal: effect of the stimulation waveform, detection system, and current amplitude using Hybrid stimulation technique». In: *IEEE Transactions on neural systems and rehabilitation engineering* 11 (2003), pp. 407–415 (cit. on p. 37).

[20] G. Anastasi et al. *Trattato di anatomia umana sistemica e funzionale*. Milano: Edi.Ermes, 2020 (cit. on p. 38).

[21] I. Barajon et al. *Anatomia umana topografica*. Milano: Edi.Ermes, 2019 (cit. on p. 39).

[22] Autodesk. *Inventor professional 2024*. Version 2024.1. Oct. 8, 2023 (cit. on p. 42).

[23] *Sensore (cella) di carico 10 kg max*. PintoElettronica. 2023. URL: `https://www.pintoelettronica.com/altro-sensore-cella-di-carico-10-kg-max.1.5.154.gp.291.uw` (cit. on p. 42).

[24] Arduino. *UNO rev 3*. 2023. URL: `https://store.arduino.cc/products/arduino-uno-rev3` (cit. on p. 42).

[25] The MathWorks Inc. *MATLAB R2023b*. Version 23.2.0.2459199. Nov. 29, 2023 (cit. on p. 42).

[26] Nicholas Giacoboni. *Basic Custom Arduino Library for HX711*. Version 3.0.0.1. May 9, 2024. URL: https://www.mathworks.com/matlabcentral/fileexchange/66641-basic-custom-arduino-library-for-hx711 (cit. on p. 42).

[27] Mesin L. Raggi M. Boccia G. «Reduction of crosstalk in the electromyogram: experimental validation of the optimal spatio-temporal filter». In: *IEEE Access* 11 (2023), pp. 112075–112084 (cit. on p. 42).

[28] Patla A.E. Fuglevand A.J. Winter D.A. «Models of recruitment and rate coding organization in motor-unit pools». In: *Journal of neurophysiology* 70 (1993), pp. 2470–2488 (cit. on p. 44).

[29] Santo Neto H. et al. «Number and size of motor units in thenar muscles». In: *Clinical anatomy* 17 (2004), pp. 308–311 (cit. on p. 45).

[30] Clamann H.P. Kukulka C. G. «Comparison of the recruitment and discharge properties of motor units in human brachial biceps and adductor pollicis in isometric contractions». In: *Brain research* 219 (1981), pp. 45–55 (cit. on p. 45).

[31] Gazzoni D. Farina D. et al. «Adjustments differ among low-threshold motor units during intermittent, isometric contractions». In: *J Neurophysiol.* 10 (2009), pp. 350–359 (cit. on p. 45).

[32] Woods J.J. Bellemare F. et al. «Motor units discharge rates in maximal voluntary contractions of three human muscles». In: *Journal of Neurophysiology* 50 (1983), pp. 1380–1392 (cit. on p. 45).

[33] McComas A.J. Kopec J. Delbeke J. «Refractory period studies in a human neuromuscular preparation». In: *J Neurol Neurosurg Psychiatry* 41 (1978), pp. 54–64 (cit. on p. 45).

[34] Gandevia S.C. Herbert R.D. «Twitch interpolation in human muscles: mechanisms and implications for measurement of voluntary activation». In: *J Neurophysiol* 82 (1999), pp. 2271–2283 (cit. on p. 46).

[35] Estigoni H.E. et al. «Evoked EMG versus muscle torque during fatiguing functional electrical stimulation-evoked muscle contractions and short-term recovery in individuals with spinal cord injury». In: *Sensor* 14 (2014), pp. 22907–22920 (cit. on p. 47).

[36] Dmitry Kaplan. *Knee point*. Version 1.1.0.0. Feb. 16, 2012. URL: https://www.mathworks.com/matlabcentral/fileexchange/35094-knee-point (cit. on p. 48).

[37] Kevin Arvai. *Kneed*. Version 0.8.5. July 19, 2023. URL: https://pypi.org/project/kneed/ (cit. on p. 48).

[38] *DS7A DS7AH High Voltage Constant Current Stimulators*. Digitimer. 2019. URL: https://www.digitimer.com/wp-content/uploads/research-electrophysiology/stimulators/DS7A-&-DS7AH-HV-Current-Stimulator/DS7A-DS7AH-HV-Current-Stimulator.pdf (cit. on p. 50).

[39] *EMG-16*. Prima Biomedical Sport. 2004. URL: http://web.tiscali.it/ottino/EMG-16.htm (cit. on p. 50).

[40] Meldrum D. et al. «Maximum voluntary isometric contraction: Reference values and clinical application». In: *Informa healthcare* 8 (2007), pp. 47–55 (cit. on p. 51).

[41] Alanazy M.H. «Clinical and electrophysiological evaluation of carpal tunnel syndrome: approach and pitfalls». In: *Neurosciences* 22 (2017), pp. 169–180 (cit. on p. 51).

[42] Jefferys J.G.R. Merrill D.R. Bikson M. «Electrical stimulation of excitable tissue: design of efficacious and safe protocols». In: *Journal of neuroscience methods* 141 (2005), pp. 171–198 (cit. on p. 52).

[43] D.R. Nogueira D.V. et al. «Effect of the rest interval duration between contractions on muscle fatigue». In: *Biomed eng online* 11 (2012), pp. 11–89 (cit. on p. 52).

[44] Wim van Drongelen. *Signal Processing for Neuroscientists*. Cambridge, Massachusetts: Academic Press, 2007 (cit. on p. 54).

[45] Conway D. Harper N.J.N. Greer R. «Neuromuscular monitoring in intensive care patients: milliamperage requirements for supramaximal stimulation». In: *BJA: British Journal of Anaesthesia* 87 (2001), pp. 625–627 (cit. on p. 56).

[46] Faghri P. D. Vromans M. «Functional electrical stimulation-induced muscular fatigue: Effect of fiber composition and stimulation frequency on rate of fatigue development». In: *J Electromyogr Kinesiol* 38 (2017), pp. 67–72 (cit. on p. 57).

[47] McComas A.J. Hicks A. Fenton J. «M wave potentiation during and after muscle activity». In: *J Appl Physiol* 66 (1989), pp. 2606–2610 (cit. on p. 57).

[48] Popovic M.R. Thrasher A. Graham G.M. «Reducing muscle fatigue due to functional electrical stimulation using random modulation of stimulation parameters». In: *Artif Organs.* 29 (2005), pp. 453–458 (cit. on p. 70).

[49] Zhiyuan L. Zong Y. et al. «MScanFit motor unit number estimation of abductor pollicis brevis: Findings from different experimental parameters». In: *Aging Neurosci.* 14 (2022), pp. 1–7 (cit. on p. 70).